were purified from bacteria as described previously (36). HCR6 (1b) RdRp with the mutation L245A [RdRp(L245A)] or I253A [RdRp(I253A)] or the double mutation L245A and I253A [RdRp(L245A/I253A)]; JFH1 (2a) RdRp with the mutation(s) A242C/S244D, A242, S244D, or T251Q; J6CF (2a) RdRp with the mutation(s) R241Q, S244D, or R241Q/S244D; and H77 (1a) RdRp(A238S/Q248E) were introduced using an *in vitro* mutagenesis kit (Stratagene) and the oligonucleotides listed in Table S1 in the supplemental material. HCR6 (1b) His_6-tagged RdRp(L245A/I253A) was removed from pET21b/KM (36) and cloned into the BamHI/XhoI site of pGEX-6P-3 (GE), resulting in pGEXHCVHCR6RdRp(L245A/I253A).

***In vitro* HCV transcription.** *In vitro* HCV transcription was performed as described previously (36). Briefly, following 30 min of preincubation without ATP, CTP, or UTP, 100 nM HCV RdRp was incubated in 50 mM Tris-HCl (pH 8.0), 200 mM monopotassium glutamate, 3.5 mM $MnCl_2$, 1 mM dithiothreitol (DTT), 0.5 mM GTP, 50 μM ATP, 50 μM CTP, 5 μM [α-^{32}P]UTP, 200 nM RNA template (SL12-1S), 100 U/ml human placental RNase inhibitor, and the lipid (amount indicated below) at 29°C for 90 min. ^{32}P-labeled RNA products were subjected to 6% polyacrylamide gel electrophoresis (PAGE) containing 8 M urea. The resulting autoradiograph was analyzed with a Typhoon Trio plus image analyzer (GE).

RNA filter binding assay. An RNA filter binding assay was performed as described previously (36). Briefly, 100 nM HCV RdRp and 100 nM ^{32}P-labeled RNA template (SL12-1S) were incubated with or without 0.01 mg/ml egg yolk sphingomyelin in 25 μl of 50 mM Tris-HCl (pH 7.5), 200 mM monopotassium glutamate, 3.5 mM $MnCl_2$, and 1 mM DTT at 29°C for 30 min. After incubation, the solutions were diluted with 0.5 ml of TE (50 mM Tris-HCl [pH 7.5], 1 mM EDTA) buffer and filtered through nitrocellulose membranes (0.45-μm pore size; Millipore). The filter was washed five times with TE buffer, and the bound radioisotope was analyzed by Typhoon Trio plus after being dried.

Enzyme-linked immunosorbent assay (ELISA). Ninety-six-well microtiter plates (Corning) were coated with 250 ng of egg yolk sphingomyelin in ethanol by evaporation at room temperature. After the wells were blocked with phosphate-buffered saline (PBS) and 3% bovine serum albumin (BSA), they were incubated with 1 pmol of the HCV RdRp of HCR6 (1b) wild type (wt) or L245A, I253A, or L245A/I253A mutant; NN (1b); H77 (1a); RMT (1a); J6CF (2a); or JFH1 (2a) wt or A242C/S244D, A242, S244D, or T251Q mutant in Tris-buffered saline (50 mM Tris-HCl [pH 7.5] and 150 mM NaCl) for 1.5 h at room temperature. After being blocked with 3% BSA, the bound HCV RdRp was detected by adding rabbit anti-HCV RdRp serum (1:5,000) (see Fig. S1 in the supplemental material) (17) before incubation with a horseradish peroxidase (HRP)-conjugated anti-rabbit IgG antibody (1:5,000; Southern Biotech). The optical density at 450 nm (OD_{450}) was measured with a Spectra Max 190 spectrophotometer (Molecular Devices) using a TMB (3,3′,5,5′-tetramethylbenzidine) Liquid Substrate System (Sigma).

HCV subgenomic replicon. A D244S mutation was introduced into the HCV strain NN (1b) subgenomic replicon pLMH14 (35), resulting in pLMH(NN)5B(D244S) [where 5B(D244S) is the NS5B protein with the mutation D244S]. The A242C/S244D mutation was introduced into the HCV JFH1 (2a) replicon, pSGR-JFH1/luc (25), resulting in pSGR-JFH1/luc5B(A242C/S244D). The HpaI and XbaI fragment of pSGR-JFH1 (18) was replaced with that of pSGR-JFH1/luc5B(A242C/S244D), resulting in pSGR-JFH15B(A242C/S244D). The A238S/Q248E mutation was introduced into HCV H77 (1a) replicon pHCVrep13(S2204I)/Neo (7) after the neomycin gene was replaced by the firefly luciferase gene [pH77(I)/luc] by insertion of AflII and AscI sites (see Table S1 in the supplemental material), resulting in pH77(I)/luc5B(A238S/Q248E). Subgenomic replicon RNA was transcribed *in vitro* by T7 RNA polymerase using MegaScript (Ambion) after the replicon plasmids were linearized by XbaI (strain NN and JFH1 replicons) or HpaI (strain H77 replicon). Subgenomic replicon RNA was stored at −80°C after being purified by phenol-chloroform extraction and ethanol precipitation.

Replicon assay with myriocin. Huh7.5.1 cells were kindly provided by F. Chisari and were maintained in Dulbecco's modified Eagle's medium (DMEM; Gibco) with 10% fetal bovine serum (FBS; Gibco) (38). HCV replicon RNA (10 μg) was transfected into 4×10^6 Huh7.5.1 cells (1×10^7/ml) in OptiMEM I (Gibco) by electroporation (GenePulser Xcell; Bio-Rad) at 270 V, 100 Ω, and 950 μF. After transfection, the cells were plated in 12-well plates incubated in DMEM–10% FBS. At 6 h after transfection, cells were treated with 0, 5, and 50 nM myriocin. At 4, 54, and 78 h after transfection (48 and 72 h after myriocin treatment), the cells were harvested, and luciferase activity was measured using a Dual-Glo luciferase assay kit and a GloMax 96 Microplate Luminometer (Promega). Luciferase activity was normalized against the activity at 4 h after transfection (26).

HCV JFH1 wt and NS5B(A242C/S244D) replicon cells. Huh7/scr cells were kindly provided by F. Chisari of the Scripps Research Institute and were maintained in Dulbecco's modified Eagle's medium (Gibco) with 10% fetal bovine serum (Gibco). RNA (10 μg each) from SGR-JFH1 and SGR-JFH1 with the mutations A242C/S244D in NS5B [NS5B(A242C/S244D) was transfected into 4×10^6 Huh7/scr cells (1×10^7/ml) in OptiMEM I (GIBCO) by electroporation (GenePulser Xcell; Bio-Rad) at 270 V, 100 Ω, and 950 μF. After transfection, the cells were plated in 10-cm dishes and incubated in DMEM–10% FBS with 1.0 and 0.5 mg/ml G418 (Gibco). JFH1 wt and NS5B(A242C/S244D) replicon cells were maintained in DMEM–10% FBS and 0.5 mg/ml G418.

Membrane floating assay. JFH1 wt and NS5B(A242C/S244D) replicon cells were suspended in two packed cell volumes of hypotonic buffer (10 mM HEPES-NaOH [pH 7.6], 10 mM KCl, 1.5 mM $MgCl_2$, 2 mM DTT, and 1 tablet/25 ml of EDTA-free protease inhibitor cocktail tablets [Roche]) and disrupted by 30 strokes of homogenization in a Dounce homogenizer using a tight-fitting pestle at 4°C. After nuclei were removed by centrifugation at 2,000 rpm for 10 min at 4°C, the supernatant (postnuclear supernatant [PNS]) was treated with 1% Triton X-100 in TNE buffer (25 mM Tris-HCl [pH 7.6] 150 mM NaCl, 1 mM EDTA) for 30 min on ice. The lysates were supplemented with 40% sucrose and centrifuged at 38,000 rpm in a Beckman SW41 Ti rotor (Beckman Coulter) overlaid with 30% and 10% sucrose in TNE buffer at 4°C for 14 h.

Western blotting. Western blotting using anti-HCV RdRp (17), rabbit anti-NS3 (32), anti-NS5A (16) and anti-caveolin-2 was performed as previously published (17).

Reagent. Egg yolk sphingomyelin, cholesterol phosphocholine, myriocin, and rabbit anti-caveolin-2 antibodies were purchased from Sigma. Hexanoyl sphingomyelin, C_6-ceramide, C_8-β-D-glucosyl ceramide, and C_8-β-D-lactosyl ceramide were purchased from Avanti Polar Lipids. [α-^{32}P]UTP was purchased from New England Nuclear.

Statistical analysis. Significant differences were evaluated using *P* values calculated from a Student's *t* test.

Nucleotide sequence accession number. The sequence of HCV RMT has been deposited in the GenBank under accession number AB520610.

RESULTS

Sphingomyelin activation of HCV RNA polymerases of various genotypes. There are several sequence variations in the sphingomyelin binding domain (SBD; amino acids 231 to 260 of HCV RdRp) among HCV genotypes (see Fig. 7A). In order to compare the RdRps of different genotypes of HCV, we purified RdRp from genotypes 1b (strains HCR6, NN, and Con1), 1a (H77 and MRT), and 2a (JFH1 and J6CF) (see Fig. S2 in the supplemental material). First, the effect of ethanol on HCV HCR6 (1b) RdRp transcription was examined because lipids were suspended in ethanol before they were added to the HCV transcription reaction mixture. We found that 2% ethanol did not inhibit HCV transcription (see Fig. S3 in the supplemental material); therefore, all subsequent experiments were performed using less than 2% ethanol.

The kinetics of sphingomyelin activation were analyzed using egg yolk sphingomyelin for HCR6 (1b) RdRp wt (Fig. 1A) and subtype 2a (JFH1 and J6CF) RdRps (Fig. 1B), and *N*-hexanoyl-D-*erythro*-sphingosylphosphorylcholine (hexanoyl sphingomyelin) was used for HCR6 (1b) RdRp wt (Fig. 1C) and subtype 1a (H77 and RMT) RdRps (Fig. 1D). The egg yolk sphingomyelin activation curve of HCR6 (1b) RdRp wt at low concentrations (<0.01 mg/ml) was sigmoid. The transcription activity of HCR6 (1b) RdRp wt increased in a dose-dependent manner. It was activated 11-fold at 0.01 mg/ml and then plateaued (14-fold activation) at 0.1 mg/ml. However, JFH1 (2a) and J6CF (2a) RdRps were activated 2.5-fold and 2.2-fold, respectively, at 0.01 mg/ml sphingomyelin, at which point they plateaued.

Egg yolk sphingomyelin is a mixture. In order to obtain the optimal molar ratio for sphingomyelin activation of HCR6 (1b)

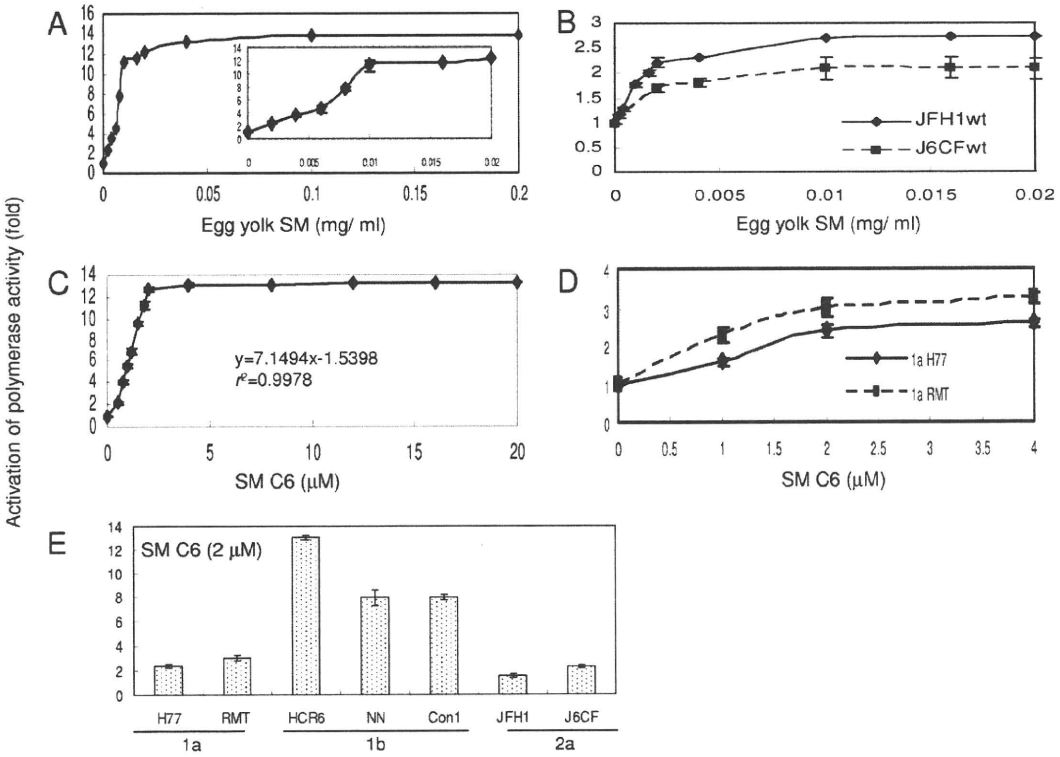

FIG. 1. Sphingomyelin activation of HCV RNA polymerases. (A) Activation kinetics of HCV HCR6 (1b) RdRp wt by egg yolk sphingomyelin (SM). The inset shows activation produced by 0 to 0.02 mg/ml egg yolk sphingomyelin. Activation kinetics of HCV 2a (JFH1 and J6CF) RdRps by egg yolk sphingomyelin (B) and of HCV HCR6 (1b) RdRp wt by hexanoyl sphingomyelin (SM C6) (C). In panel C, the first order of the graph was fitted by linear regression; the calculated equation is indicated in the graph. (D) Activation kinetics of HCV 1a (H77 and RMT) RdRps by hexanoyl sphingomyelin. (E) Activation effect of hexanoyl sphingomyelin on HCV RdRp of various genotypes. HCV RdRp (100 nM) was incubated with or without 2 μM SM C6. The names of the RdRps are indicated below the graph. Mean ± standard deviation of the activation ratio was calculated from three independent experiments.

RdRp wt, its activation kinetics were calculated using hexanoyl sphingomyelin (Fig. 1C, SM C6). The equation for the first-order ratio of hexanoyl sphingomyelin activation according to linear regression fitting was as follows: $y = 7.1494x - 1.5398$, where y is the activation ratio and x is the sphingomyelin concentration ($r^2 = 0.9978$). RdRp activation had almost plateaued at 2 μM hexanoyl sphingomyelin. The activation kinetics of JFH1 (2a) and J6CF (2a) RdRps in egg yolk sphingomyelin were biphasic and plateaued at 0.01 mg/ml. Those of RMT (1a) and H77 (1a) RdRps in hexanoyl sphingomyelin were also biphasic and plateaued at 2 μM. The curve of the first order was fitted by linear regression. The molar ratio of RdRp to hexanoyl sphingomyelin at its plateau was calculated as 1:20.

Because RdRp activation had almost plateaued at 2 μM hexanoyl sphingomyelin, we compared the effect of sphingomyelin on 100 M concentrations of RNA polymerases of the HCV 1a, 1b, and 2a genotypes using 2 μM hexanoyl sphingomyelin (Fig. 1E and Table 1).

Helix-turn-helix structure for sphingomyelin binding and activation. Sphingomyelin binds to the SBD peptide (see HCV SBD in Fig. 7) (29). Initially, we tested whether SBD was the sphingomyelin binding site in HCV RdRp by ELISA (Fig. 2A and Table 1). When the L245 and I253 residues of the SBD peptide were mutated to A, sphingomyelin binding activity was lost (29). We introduced the same mutations in HCV HCR6 (1b) RdRp and purified HCR6 (1b) RdRp with mutations L245A, I253A, and L245A/I253A. Because the C-terminal His-tagged HCR6 RdRp(L245A/I253A) was not soluble, it was solubilized by tagging of glutathione *S*-transferase (GST) sequence at the N terminus but lost polymerase activity. As the L245A/I253A mutant had lost its polymerase activity, polymerase activation was tested only for L245A and I253A (Fig. 2B and Table 1). These results confirmed that SBD located in the finger domain (residues 230E to 263G) successfully achieved sphingomyelin binding in HCV RdRp and that sphingomyelin did not bind to the SBD when the helix-turn-helix structure had been destroyed by the L245A or I253A mutation (29).

The sphingomyelin binding activities of genotype 1a and 2a RdRps were also tested (Fig. 2 and Table 1). Both JFH1 and J6CF were tested for genotype 2a because J6CF (2a) RdRp had an additional amino acid difference at position 241 in the SBD, and its sphingomyelin binding activity was very low (Fig. 2A and 7A; Table 1). J6CF (2a) RdRp(R241Q) showed the same sphingomyelin binding activity as HCR6 (1b) RdRp wt, indicating that 241Q was the critical amino acid for sphingomyelin binding. J6CF (2a) RdRp(S244D) and RdRp(R241Q/S244D) also showed higher sphingomyelin binding activity

TABLE 1. Summary of sphingomyelin activation of HCV RNA polymerase activities

Parameter	Value for the parameter by RdRp genotype, strain, and variant[a]																				
	1b							1a				2a									
	HCR6					NN	Con1	RMT	H77			J6CF				JFH1					
	wt	L245A	I253A	L245A/I253A	D244S	wt	wt	wt	wt	A238S/Q248E	wt	R241Q	S244D	R241Q/S244D	wt	A242C	S244D	A242C/S244D	T251Q
SM binding (%)[b]	100	24.3	30.8	15.5	78.7	93.4	117	144	86.7	82.5	19.3	118	53.1	80.2	70.4	75.5	93.1	92.4	80.7
Activation of polymerase (n-fold)[c]	13.0 (11.2)[d]	(2.8)[d]	(2.5)[d]	ND	3.6	7.9	7.9	3.0	2.0	8.1	2.3	4.3	5.6	3.4	1.6	1.0	3.1	4.4	1.8
Activation of RNA binding (n-fold)[c]	4.5	2.6	1.7	ND	1.9	ND	ND	ND	1.4	3.3	1.5	3.6	3.2	1.7	1.3	ND	ND	1.4	ND

[a] Numbers were averaged from three independent experiments. ND, not done.
[b] Egg yolk sphingomyelin (SM; 250 ng) was used.
[c] Hexanoyl sphingomyelin (2 μM) was used.
[d] Egg yolk sphingomyelin (0.01 mg/ml) was used.

than the wt ($P < 0.001$) but lower binding than the R241Q mutant. However, S244D showed higher RdRp activation than R241Q ($P < 0.005$), while the RdRp activation ratio of the double mutant (R241Q/S244D) was lower than that of S244D or R241Q, although all of them activated RdRp with sphingomyelin ($P < 0.005$) (Fig. 2A and C and Table 1). For JFH1, when the JFH1 RdRp SBD was modified (A242C/S244D) to allow it to bind with more sphingomyelin than the wt ($P < 0.005$), the mutant JFH1 RdRp(A242C/S244D) was activated more than the wt by sphingomyelin ($P < 0.005$) (Fig. 2A and C; Table 1). The sphingomyelin binding activity of JFH1 RdRp(T251Q) was 80.7% of that of HCR6 (1b), and its activation ratio was 1.8-fold. These results agree that SBD is both the sphingomyelin activation and binding domain and that the domains for these two activities are somehow different.

We determined which amino acid, 242C or 244D, enhanced sphingomyelin binding by comparing HCR6 (1b) and JFH1 (2a) RdRps. Sphingomyelin binding of HCR6 (1b) RdRp(D244S) was 79% of that of the wt ($P < 0.005$) (Fig. 2A and Table 1), and its activation by sphingomyelin was only 3.6-fold (Fig. 2C and Table 1). The sphingomyelin binding of JFH1 (2a) RdRp(A242C) and RdRp(S244D) increased to 75.5% and 93.1%, respectively, of HCR6 (1b) RdRp wt (Fig. 2A and Table 1). This was significantly higher than that of JFH1 (2a) RdRp wt ($P < 0.005$), and the sphingomyelin activation of JFH1 (2a) RdRp(A242C) and RdRp(S244D) was increased 1.0-fold and 3.1-fold, respectively ($P < 0.005$) (Fig. 2C and Table 1). From these mutation analyses of the J6CF and JFH1 RdRps, we concluded that 244D enhanced sphingomyelin binding and RdRp activation.

HCV 1a RdRps were not activated even though sphingomyelin bound to them (Fig. 1E and 2A and Table 1). We then tried to elucidate the domains responsible for sphingomyelin activation. There are 14 amino acids (residues 19, 25, 81, 111, 120, 131, 184, 270, 272, 329, 436, 464, 487, and 540) unique to genotype 1a RdRp in the region of residues 1 to 570 and two amino acid differences unique to 1a RdRp in SBD, i.e., 238A and 248Q (see Fig. 6A). Initially, we focused on the SBD and introduced the A238S and Q248E mutations into the H77 (2a) RdRp SBD (Fig. 2A and D and Table 1). The sphingomyelin binding activity of H77 (2a) RdRp(A238S/Q248E) was similar to that of H77 (2a) RdRp wt. The sphingomyelin activation ratio of H77 (2a) RdRp(A238S/Q248E) was increased 8.1-fold, leading us to conclude that these mutations are essential to sphingomyelin activation.

Effect of lipids on HCV RNA polymerase activity. In order to elucidate the structure of the lipids involved in activation of HCV RdRp, D-lactosyl-β-1,1′-*N*-octanoyl-D-*erythro*-sphingosine [C_8-lactosyl(β) ceramide], D-glucosyl-β1-17-N-octanoyl-D-*erythro*-sphingosine (C_8-β-D-glucosyl ceramide), *N*-hexanol-D-*erythro*-sphingosine (C_6-ceramide), and cholesterol were tested for their abilities to activate RdRp. The relative polymerase activities of 100 nM HCV HCR6 (1b) RdRp activated with 0.01 mg/ml egg yolk sphingomyelin, 2 μM hexanoyl sphingomyelin, 8 μM C_8-lactosyl(β) ceramide, 12 μM C_8-β-D-glucosyl ceramide, 12 μM C_6-ceramide, and 0.02 mg/ml cholesterol were 11.2, 13.0, 5.66, 4.19, 1.12, and 2.25 of that without lipids, respectively (Fig. 3A). The amount of lipids that gave the maximum activation was calculated from the kinetics of the lipids bound to HCR6 (1b) and JFH1 (2a) RdRps (Fig. 3B and

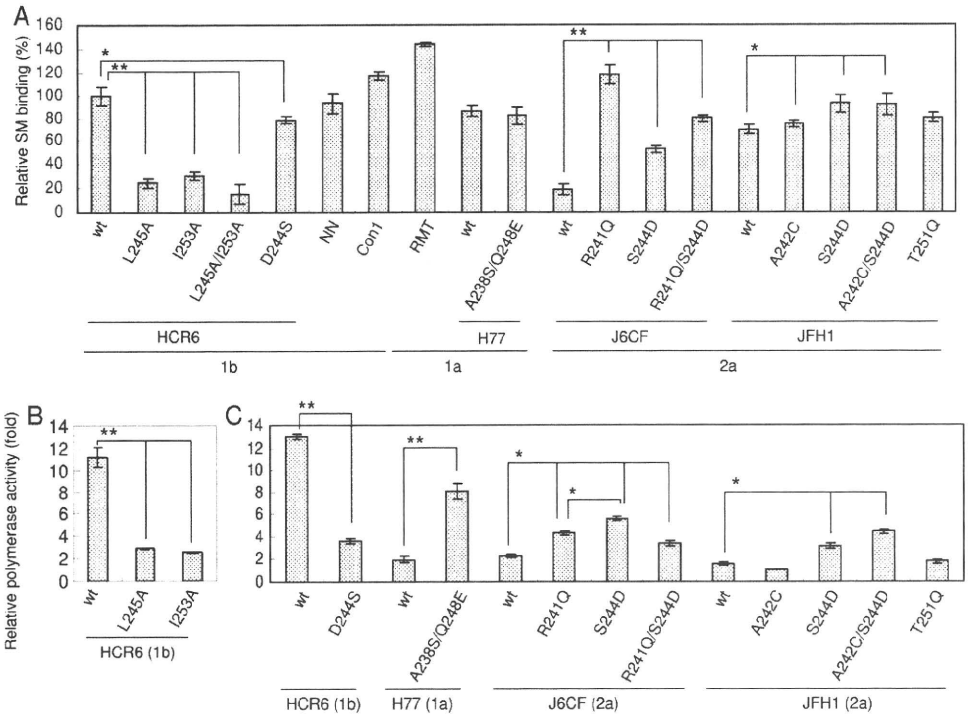

FIG. 2. Sphingomyelin binding and activation of HCV RNA polymerase sphingomyelin binding domain mutants. Names of RdRps are indicated below the graphs. (A) Egg yolk sphingomyelin (SM) binding activity relative to that of HCR6 (1b) RdRp wt. Mean ± standard deviation of the binding was calculated from three independent experiments. (B) Egg yolk sphingomyelin activation of HCR6 (1b) RdRps. RdRps (100 nM) were incubated with or without 0.01 mg/ml egg yolk sphingomyelin. (C) Hexanoyl sphingomyelin activation of the RdRps (RdRp names are indicated below the graphs). HCV RdRps (100 nM) were incubated with or without 2 μM hexanoyl sphingomyelin. The mean ± standard deviation of the activation ratio was calculated from three independent experiments. *, $P < 0.005$; ** $P < 0.001$.

C). C_8-lactosyl(β) ceramide and C_8-β-D-glucosyl ceramide activated HCR6 (1b) RdRp compared with the linear regression kinetics of the reaction with hexanoyl sphingomyelin as it plateaued (Fig. 1C and 3B). Cholesterol activated HCR6 (1b) RdRp slightly but did not activate JFH1 (2a) RdRp (Fig. 3C). We therefore concluded that the phosphocholine of sphingomyelin bound to the SBD of HCV RdRp because the order of HCV RdRp activation was hexanoyl sphingomyelin > C_8-lactosyl(β) ceramide > C_8-β-D-glucosyl ceramide, and C_6-ceramide did not activate HCV HCR6 (1b) RdRp. The polarity of the phosphocholine of sphingomyelin is important for HCV RdRp activation (see Fig. S5 in the supplemental material).

In order to test whether phosphocholine activated HCV RdRp (Fig. 3D), HCR6 (1b) RdRp was incubated with 0.4, 2, 20, 100, and 400 μg and 2, 4, 11, 54, and 100 mg of phosphocholine. Up to 400 μg of phosphocholine did not affect RdRp activity, but more than 2 mg of phosphocholine inhibited RdRp activity.

Effect of sphingomyelin on the template RNA binding of HCV RNA polymerase. The mechanism of HCV RdRp activation was analyzed. RNA polymerase changes its conformation throughout the different transcription steps, and template binding is the first step of transcription (9). Therefore, the effect of sphingomyelin on template RNA binding activity was tested (Fig. 4A and Table 1). Sphingomyelin enhanced the template RNA binding of HCR6 (1b) RdRp wt but not that of JFH1 (2a), H6CF (2a), or H77 (1a) wt RdRp. When the A238S/Q248E mutation was introduced into H77 (1a) RdRp, the RNA binding was enhanced. J6CF (2a) RdRp R241Q and S244D mutants showed similar enhancement of RNA binding, but the R241Q/S244D double mutant did not. The activation effect of RNA binding of HCR6 (1b) RdRp mutants L245A, I253A, and D244S was lower than that of RdRp wt. JFH1 (2a) RdRp wt and RdRp(A242C/S244D) showed similar RNA binding activation levels. Based on a comparison of the sphingomyelin activation of HCR6 (1b) RdRp wt and its mutants which lost sphingomyelin binding with J6CF (2a) RdRp wt and the R241Q and S244D mutants and H77 (1a) RdRp wt and the A238S/Q248E mutant, we concluded that polymerase activation by sphingomyelin was induced mainly via activation of the template RNA binding of RdRp. RNA binding activity of JFH1 (2a) RdRp wt and RdRp(A242C/S244D) was almost saturated because RNA binding of these RdRps was not activated by sphingomyelin (see Fig. S4 in the supplemental material).

HCV RdRp has to be bound with sphingomyelin before or at the same time as it binds to template RNA. After RdRp had bound to the template RNA, sphingomyelin did not enhance template RNA binding strongly (Fig. 4B).

Effect of the sphingomyelin binding domain mutations for HCV replicon activity with myriocin. In order to confirm sphingomyelin activation of HCV polymerase activity in a viral replication system, HCV replicon activity of the loss-of-function mutant HCV NN (1b) NS5B(D244S) and the gain-of-

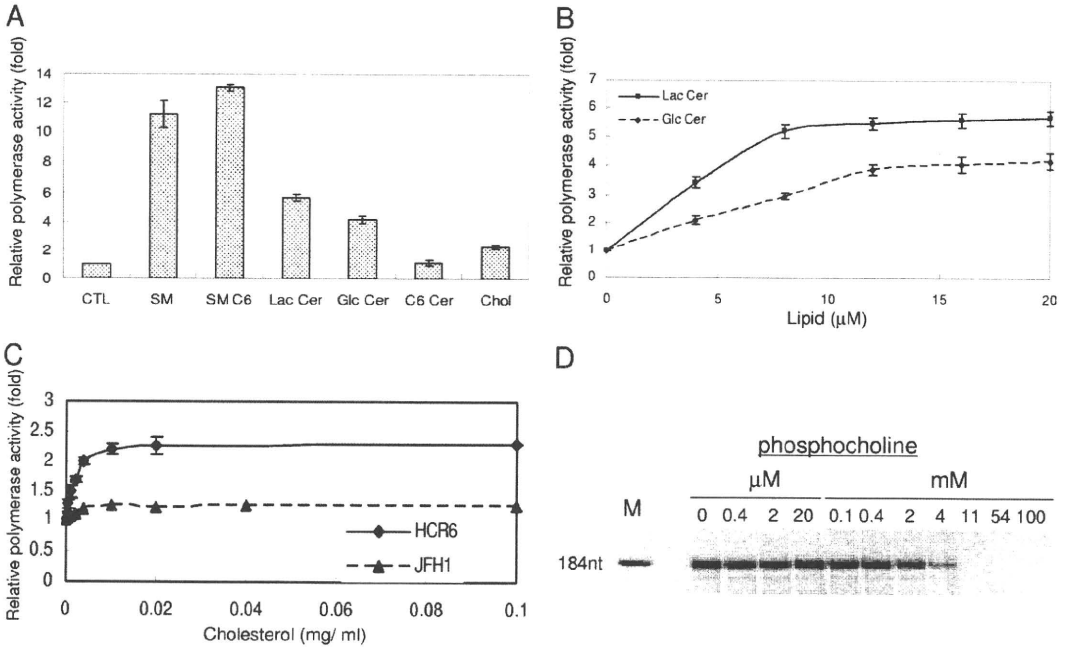

FIG. 3. HCV RNA polymerase activation effect of lipids. (A) Lipid activation of HCR6 (1b) RdRp wt. HCV HCR6 (1b) RdRp wt (100 nM) was incubated with or without (control [CTL]) 0.01 mg/ml egg yolk sphingomyelin (SM), 2 μM hexanoyl sphingomyelin (SM C6), 8 μM C_8-lactosyl(β) ceramide (Lac Cer), 12 μM C_8-β-D-glucosyl ceramide (Glc Cer), 12 μM C_6-ceramide (C6 Cer), or 0.02 mg/ml cholesterol (chol). (B) Activation kinetics of C_8-lactosyl(β) ceramide (Lac Cer) and C_8-β-D-glucosyl ceramide (Glc Cer) on HCR6 (1) RdRp. (C) Activation kinetics of cholesterol on HCR6 (1b) and JFH1 (12a) RdRps. (D) The effect of phosphocholine on HCR6 (1b) RdRp. The mean ± standard deviation of the activation ratio was calculated from three independent experiments.

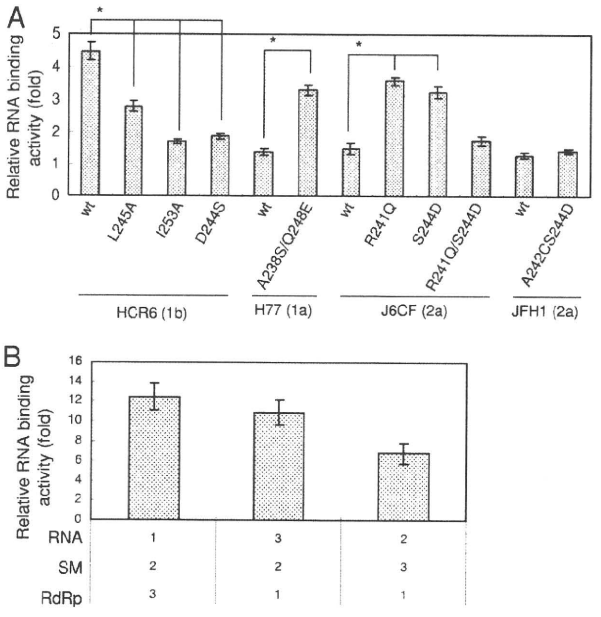

FIG. 4. Sphingomyelin activation of the RNA binding activity of HCV RNA polymerase. (A) Sphingomyelin activation of RNA filter binding of HCV RdRps (RdRp names are indicated below the graph). RdRps and ^{32}P-labeled RNA template (SL12-1S) were incubated with or without egg yolk sphingomyelin (SM), before filtration. (B) Effect of the order of sphingomyelin treatment. Numbers below the graph indicate the order in which the reagents were added. The graph represents the ratio to RNA binding without sphingomyelin. The mean ± standard deviation of the activation ratio was calculated from three independent experiments. *, $P < 0.01$.

function mutants H77 (1a) NS5B(A238S/Q248E) and JFH1 (2a) NS5B(A242C/S244D) were compared with 5 and 50 nM myriocin treatment for 72 h (Fig. 5).

First, HCV replicon activity was compared as the relative luciferase activity (Fig. 5A). Both JFH1 (2a) wt and NS5B(A242C/S244D) replicons showed similar and strong replicon activity ($133 \times 10^3 \pm 12 \times 10^3$ and $138 \times 10^3 \pm 8.5 \times 10^3$, respectively). JFH1 (2a) wt replicon was resistant to myriocin treatment, as reported by Aizaki et al. using other SPT inhibitors (3). The JFH1 (2a) NS5B(A242C/S244D) replicon became sensitive to myriocin but still showed higher replicon activity than NN (1b) or H77 (1a) replicons even at 50 nM myriocin.

To analyze the effect of mutations precisely, the replicon activity relative to each wt strain was compared (Fig. 5B). The JFH1 (2a) wt replicon with 50 nM myriocin showed the same luciferase activity as the wt without myriocin (102% ± 9.6%). JFH1 (2a) NS5B(A242C/S244D) replicon activity was the same as that of the wt without myriocin (103% ± 12%); with 5 nM myriocin it was 84.1% ± 6.6% of the wt level, but with 50 nM myriocin it was 70.3% ± 5.3% of the wt level, which was significantly lower ($P < 0.01$). NN (1b) wt replicon activity was 45.3% ± 6.6% with 5 nM myriocin and 21.7% ± 2.9% with 50 nM myriocin relative to the wt level without myriocin. NN (1b) NS5B(D244S) replicon activity was 72.2% ± 12% without myriocin ($P < 0.05$), 44.0% ± 7.4% with 5 nM myriocin, and 38.1% ± 4.2% with 50 nM myriocin relative to wt level without myriocin, which was significantly higher ($P < 0.01$). Thus, NN (1b) NS5B(D244S) showed lower replicon activity than the wt

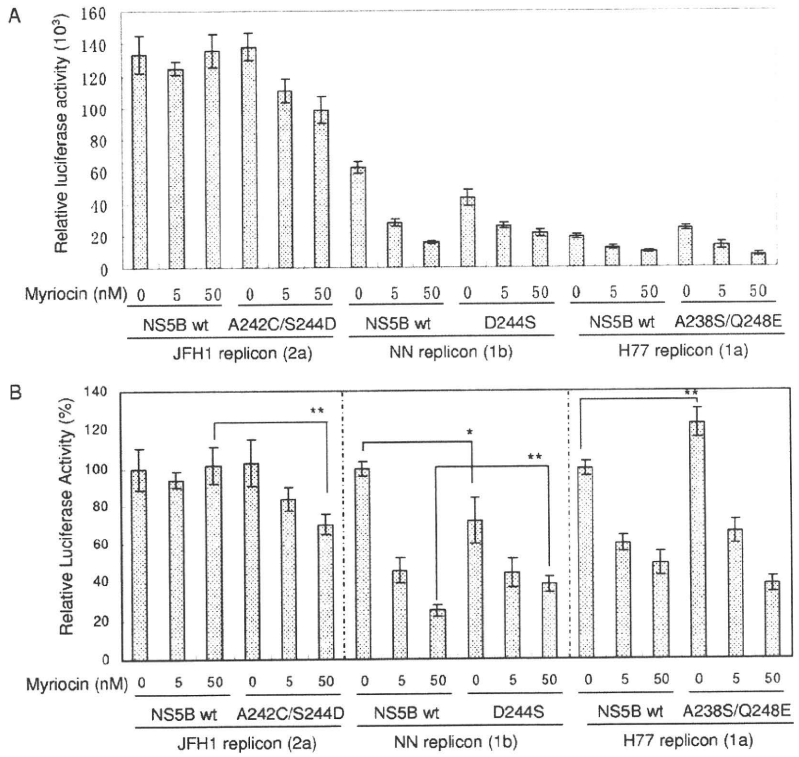

FIG. 5. Myriocin inhibition of HCV replicon activity. Huh7.5.1 cells were incubated with myriocin after transfection with the HCV replicons indicated below the graphs. Means ± standard deviations of the relative luciferase activity at 72 h after myriocin treatment compared to activity at 4 h after transfection (A) and to that of each wt without myriocin (B) were calculated from three independent measurements. *, $P < 0.05$; ** $P < 0.01$.

and was less sensitive to myriocin than the wt. H77 (1a) wt replicon activity was 59.9% ± 4.2% with 5 nM myriocin and 49.2% ± 6.4% with 50 nM myriocin relative to the wt level without myriocin. H77 (1a) NS5B(A238S/Q248E) replicon activity was 123% ± 7.1% without myriocin ($P < 0.01$), 66.1% ± 6.3% with 5 nM myriocin, and 38.0% ± 4.1% with 50 nM myriocin relative to wt level without myriocin. Both H77 (1a) wt and NS5B(A238S/Q248E) replicons were sensitive to myriocin, and the replicon activity of NS5B(A238S/Q248E) was higher than that of the wt.

JFH1 (2a) RdRp(A242C/S244D) localized in the DRM fractions. Myriocin sensitivity of JFH1 (2a) NS5B(A242C/S244D) replicon indicates the importance of 244D in JFH1 NS5B for sphingomyelin binding. To further confirm the role of 244D for recruitment of HCV RdRp to the detergent-resistant membrane (DRM), where the HCV replication complex exists, we compared the distribution of NS5A and NS5B of JFH1 (2a) wt and NS5B(A242C/S244D) in their replicon cells by sucrose density gradient centrifugation of the DRM (Fig. 6). NS5A proteins of both JFH1 (2a) wt and NS5B(A242C/S244D) replicons localized in the DRM fraction where caveolin-2 was present (11, 27), but most of NS5B wt localized in the Triton-soluble fractions. NS5B of JFH1 (2a) NS5B(A242C/S244D) replicon was shifted to the DRM fraction from the soluble fraction. The shift of NS5B(A242C/S244D) localization into the DRM demonstrated that SBD was the DRM localization domain of NS5B and that residue 244D was important for this localization.

DISCUSSION

Hepatitis C virus is an envelope virus, and the lipid components of the virion play important roles in HCV infectivity and virion assembly (3, 15, 20, 24). HCV replication complexes localize in lipid raft structures/DRMs in the membrane frac-

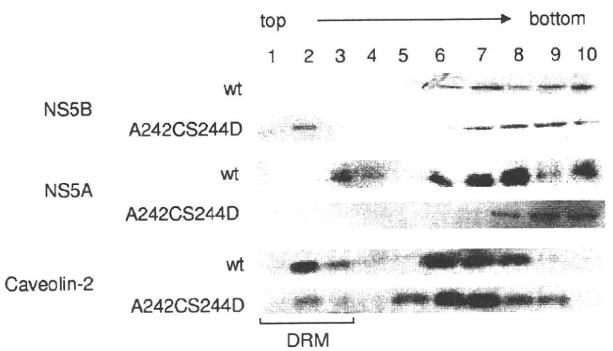

FIG. 6. Membrane floating assay of JFH1 wt and NS5B(A242C/S244D) replicon cells. The PNS fractions of HCV JFH1 (2a) wt and NS5B(A242C/S244D) replicon cells were treated with 1% Triton X-100 in TNE buffer for 30 min at 4°C and subjected to 10 to 40% sucrose gradient centrifugation in TNE buffer. Each fraction was subjected to 10% SDS-PAGE, followed by Western blotting with anti-NS5A, -NS5B, and -caveolin-2 antibodies. Fractions are numbered as indicated at the top of the panel. The DRM fractions (fractions 1 to 3) are indicated.

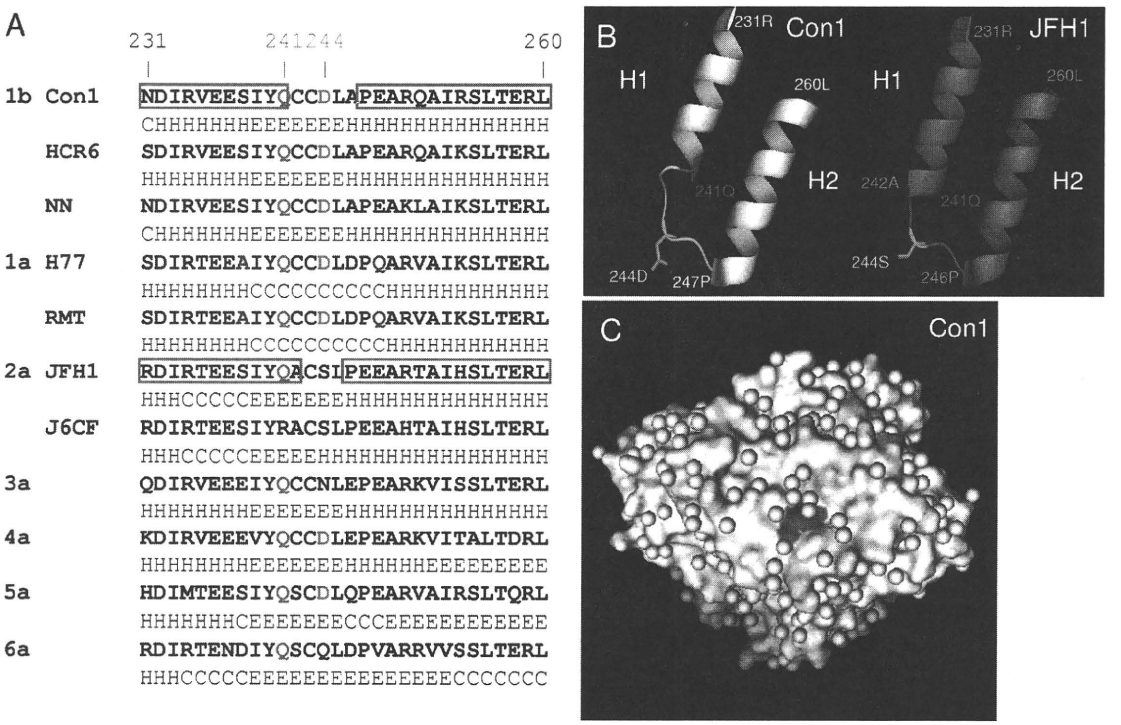

FIG. 7. Sphingomyelin binding domain (SBD) of HCV RNA polymerase. (A) The SBDs (231N to 260L) of HCV RdRps are aligned together with their secondary structure predicted by the Chou-Fasman program (10). The predicted secondary structure is indicated below the sequence as follows: H, α-helix; E, β-sheet; and C, coil. The α-helix structures of HCV Con1 (1b) RdRp and JFH1 (2a) RdRp are boxed in red. Residues 241Q and 244D are indicated in red and green, respectively. The 238A and 248E of the H77 and RMT (1a) RdRps are indicated in purple. GenBank accession numbers of HCV genotypes 3a, 4a, 5a, and 6a are GU814263 (12), GU814265 (12), Y13184 (8), and Y12083 (1), respectively. (B) Comparison of the SBDs of HCV Con1 (1b) (yellow) and JFH1 (2a) RdRps (magenta). The starting and ending amino acids of H1 and H2 are indicated. The sphingomyelin binding site, 241Q, is indicated in red, and 244D of Con1 (1b) and 244S of JFH1 (2a) RdRp are indicated in green. (C) Surface model of HCV Con1 (1b) RdRp. SBD is indicated in yellow, and 241Q and 244D are indicated in red and green, respectively. The structures of the Con1 and JFH1 RdRps were constructed by PyMOL, version 1.1.1 (http://www.pymol.org/). PDB numbers of Con1 (1b) RdRp and JFH1 (2a) RdRp are 3FQL (14) and 3I5K (31), respectively.

tions of subgenomic replicon cells (30). Lipid rafts are composed mainly of sphingomyelin, cholesterol, and glycosphingolipids. Most reports regarding the relationship between lipids and HCV have examined virion assembly, infectivity, and the localization of HCV, but their biochemical interactions have not been reported. Our findings clearly demonstrate that sphingomyelin plays an important role not only in HCV replication complex formation and its localization but also in HCV RdRp activity.

The helix-turn-helix structure of the SBD (residues 230 to 263), which is located between RNA polymerase motifs A and B, has been proposed as the sphingomyelin binding domain of HCV RdRp (29). We compared the SBD of Con1 (1b) (Protein Data Bank [PDB] 3FQL) (14) and JFH1 (2a) (PDB 3I5K) (31) and the secondary structure of the amino acids (201 to 290) in the SBD predicted by the Chou-Fasman program (10) (Fig. 7; see also Fig. S5 in the supplemental material) because the helix structures of the SBD of Con1 (helix 1 [H1], 231N to 241Q; helix 2 [H2], 247A to 260L) and JFH1 (H1, 231R to 242A; H2, 246P to 260L) RdRp fit with those predicted by the Chou-Fasman program. The structures contributing to sphingomyelin binding and activation are H1 and H2 and the junction (turn) between the two helix structures that are similar to the human immunodeficiency virus (HIV) gp120 V3 domain, prion protein (PrP), and β-amyloid peptide (13, 22). Although Con1 (1b) RdRp has a shorter helix structure than JFH1 (2a) RdRp (Fig. 6B), the structures of their SBDs are very similar (Fig. 7; see also Fig. S5). When the helix-turn-helix structure of the SBD was destroyed (HCR6 genotype 1b RdRp mutants L245A and I253A), the RdRp lost sphingomyelin binding activity and lost its activation (Fig. 2).

In order to study the structure-function relationship of the SBD and sphingomyelin, we compared the SBD of genotype 1a, 1b and 2a RdRps and particularly focused on residue 244D in the turn and residues 241Q and 238S/248E in the helix domains. The polar amino acid 241Q and the negatively charged 244D of Con1 (1b) RdRp located on the surface of the RdRp molecule bind and interact with the positively charged choline residue of sphingomyelin (Fig. 7C; see also Fig. S5 in the supplemental material). The positively charged 241R repels the choline residue of sphingomyelin, and as a result, J6CF (a) RdRp wt did not bind to sphingomyelin. J6CF (2a) RdRp(R241Q) showed almost the same sphingomyelin binding activity as HCR6 (1b) RdRp wt. This ionic interaction between SBD and sphingomyelin agrees with the activation of lipids with different sphingosine structures and fatty acid chains (Fig. 3A). JFH1 (2a) RdRp does not interact well with sphingomyelin because it does not have the negatively charged

amino acids at the tip of its turn structure. Once its 244S was changed to D, more sphingomyelin bound to JFH1 (2a) RdRp and activated the RdRp (Fig. 2A and C). The reason for the low activation of J6CF (2a) RdRp(R241Q/S244D) is not clear. Sometimes mutations affect the entire conformation of the molecule. In conclusion, from the comparison of sphingomyelin binding and activation of HCR6 (1b), J6CF (2a), and JFH1 (2a) RdRp SBD mutants, 241Q is the essential amino acid for sphingomyelin binding in the SBD. Amino acid 244D enhanced both binding and RdRp activation.

The *in vitro* sphingomyelin binding and RdRp activation experiments indicate that sphingomyelin binding and its RdRp activation are different biochemical reactions because we found controversial activation rates for sphingomyelin binding and RdRp activation among J6CF (2a) RdRp mutants (Fig. 2). The relationship between sphingomyelin binding and the activation of polymerase activity was studied by comparing genotype 1b and 1a RdRps, both of which bind to sphingomyelin (Fig. 2). However, 1a RdRp is not activated by sphingomyelin because both of the helix structures of 1a RdRp are probably terminated at 238A and 248Q, making its helix structures shorter than those of 1b RdRp (Fig. 6A). The length of the helix structure may be essential for sphingomyelin activation because RdRp changes its structure to bind to template RNA when sphingomyelin binds to SBD (Fig. 4).

HCV RdRp changes its conformations at the early stages of transcription initiation, including the template RNA binding step (6, 9). Sphingomyelin binding is likely to change the conformation of 1b RdRp to recruit template RNA and initiate transcription efficiently. Comparison of the activation ratio of RNA binding and polymerase activity of 1b RdRp, J6CF (2a) RdRp wt and R241Q and S244D mutants, and JFH1 (2a) RdRp wt and mutant A242C/S244D suggests that steps other than RNA binding are also likely to be activated by sphingomyelin.

From a kinetic analysis of sphingomyelin activation (Fig. 1C and D), 20 sphingomyelin molecules are estimated to interact with the SBD of RdRp and activate it because sphingomyelin activation plateaued at 20 sphingomyelin molecules per HCV RdRp molecule. It is not clear whether 20 sphingomyelin molecules form a micelle or a layer structure. However, the structure of sphingomyelin is important for the activation of HCV RdRp because phosphocholine did not activate the RdRp (Fig. 3D).

To confirm these biochemical findings in HCV replication, we tested the effect of SBD mutations in HCV replicon systems with the SPT inhibitor myriocin (Fig. 5) (4, 33) because NA255 was not available. The loss-of-function mutant, HCV NN (1b) NS5B(D244S), showed lower replicon activity than NN (1b) wt and more resistance to 50 nM myriocin, which did not affect the viability of cells (4, 33), than the wt. The gain-of-function mutant, H77 (1a) NS5B(A238S/Q248E), showed higher replicon activity than H77 wt and retained myriocin sensitivity because it had the sphingomyelin binding sites 241Q and 244D. At 50 nM myriocin, another gain-of-function mutant, JFH1 (2a) NS5B(A242C/S244D), was inhibited although its activity was the same as that of JFH1 (2a) wt without myriocin because the JFH1 wt replicon had high replicon activity without myriocin (Fig. 5A). The JFH1 replicon activity may be maximal in the system; therefore, the JFH1 (2a) NS5B(A242C/S244D) replicon did not show higher activity than JFH1 (2a) wt without myriocin while H77 (1a) NS5B(A238S/Q248E) showed higher replicon activity than H77 wt.

The binding and RdRp activation activity of the amino acid 244 mutants by sphingomyelin did not differ greatly from the wt *in vitro*. However, the myriocin sensitivity of JFH1 (2a) NS5B(S244D) was demonstrated clearly. That of H77 (1a) NS5B(A238S/Q248E) indicated that sphingomyelin binding was the target of myriocin inhibition, not the sphingomyelin activation of RdRp. These data confirm the importance of 241Q, 244D, and the helix structure in SBD for HCV replication in the cells.

Sphingomyelin is the major component of the lipid raft structure/DRM where the HCV genome replicates. To confirm that the SBD is the membrane binding site of HCV RdRp, we analyzed the localization of NS5B of JFH1 (2a) wt and NS5B(A242C/S244D) replicons by membrane floating assay (Fig. 6). JFH1 (2a) NS5B wt did not localize in the DRM. However, the localization of NS5B of the JFH1 (2a) NS5B(A242C/S244D) replicon shifted to the DRM from the soluble fractions. Previously, HCV NS5B was believed to localize in the DRM by its C-terminal hydrophobic sequences (21). However, our data demonstrate that the SBD is the membrane localization domain of HCV NS5B, which agrees with the myriocin sensitivity of JFH1 (2a) NS5B(A242C/S244D) replicons (Fig. 5) and the release of HCV 1b NS5B from the DRM by another SPT inhibitor, NA255 (29).

This is the first report of RNA polymerase activation by lipids. Twenty sphingomyelin molecules interact with SBD, particularly with residues 241Q and 244D of HCV (1b) RdRp, and change the conformation of the RdRp in order to recruit RNA templates. At the same time, HCV RdRp molecules may be aligned on the sphingomyelin layer formed via interactions between the hydrocarbon chains of sphingosine and fatty acids via placement of their SBD into the layer (Fig. 7C). Consistent with previous research (3, 23, 37), our findings explain why the inhibitors of the sphingolipid biosynthetic pathway influence subgenomic replicons derived from HCV genotypes 1a and 1b but not those derived from JFH1 (2a) (Fig. 5). Most HCV isolates have 241Q in NS5B, and some of them also have 244D (Fig. 7A). These sphingomyelin interactions are new targets for the treatment of HCV.

ACKNOWLEDGMENTS

We thank C. Rice and R. Bartenshlager for the HCV H77 and Con1 plasmids, respectively. We also thank F. Chisari for Huh7.5.1 and Huh7/src cells.

This work was supported by a grant-in-aid from the Chinese Academy of Sciences (O514P51131 and KSCX1-YW-10), the Chinese 973 project (2009CB522504), and the Chinese National Science and Technology Major Project (2008ZX10002-014).

REFERENCES

1. **Adams, N. J., R. W. Chamberlain, L. A. Taylor, F. Davidson, C. K. Lin, R. M. Elliott, and P. Simmonds.** 1997. Complete coding sequence of hepatitis C virus genotype 6a. Biochem. Biophys. Res. Commun. **234**:393–396.
2. **Aizaki, H., K. J. Lee, V. M. Sung, H. Ishiko, and M. M. Lai.** 2004. Characterization of the hepatitis C virus RNA replication complex associated with lipid rafts. Virology **324**:450–461.
3. **Aizaki, H., K. Morikawa, M. Fukasawa, H. Hara, Y. Inoue, H. Tani, K. Saito, M. Nishijima, K. Hanada, Y. Matsuura, M. M. Lai, T. Miyamura, T. Wakita, and T. Suzuki.** 2008. Critical role of virion-associated cholesterol and sphingolipid in hepatitis C virus infection. J. Virol. **82**:5715–5724.
4. **Amemiya, F., S. Maekawa, Y. Itakura, A. Kanayama, A. Matsui, S. Takano, T. Yamaguchi, J. Itakura, T. Kitamura, T. Inoue, M. Sakamoto, K. Yamau-**

chi, S. Okada, A. Yamashita, N. Sakamoto, M. Itoh, and N. Enomoto. 2008. Targeting lipid metabolism in the treatment of hepatitis C virus infection. J. Infect. Dis. **197**:361–370.
5. **Binder, M., D. Quinkert, O. Bochkarova, R. Klein, N. Kezmic, R. Bartenschlager, and V. Lohmann.** 2007. Identification of determinants involved in initiation of hepatitis C virus RNA synthesis by using intergenotypic replicase chimeras. J. Virol. **81**:5270–5283.
6. **Biswal, B. K., M. M. Cherney, M. Wang, L. Chan, C. G. Yannopoulos, D. Bilimoria, O. Nicolas, J. Bedard, and M. N. James.** 2005. Crystal structures of the RNA-dependent RNA polymerase genotype 2a of hepatitis C virus reveal two conformations and suggest mechanisms of inhibition by non-nucleoside inhibitors. J. Biol. Chem. **280**:18202–18210.
7. **Blight, K. J., J. A. McKeating, J. Marcotrigiano, and C. M. Rice.** 2003. Efficient replication of hepatitis C virus genotype 1a RNAs in cell culture. J. Virol. **77**:3181–3190.
8. **Chamberlain, R. W., N. J. Adams, L. A. Taylor, P. Simmonds, and R. M. Elliott.** 1997. The complete coding sequence of hepatitis C virus genotype 5a, the predominant genotype in South Africa. Biochem. Biophys. Res. Commun. **236**:44–49.
9. **Chinnaswamy, S., I. Yarbrough, S. Palaninathan, C. T. Kumar, V. Vijayaraghavan, B. Demeler, S. M. Lemon, J. C. Sacchettini, and C. C. Kao.** 2008. A locking mechanism regulates RNA synthesis and host protein interaction by the hepatitis C virus polymerase. J. Biol. Chem. **283**:20535–20546.
10. **Chou, P. Y., and G. D. Fasman.** 1974. Prediction of protein conformation. Biochemistry **13**:222–245.
11. **Fujimoto, T., H. Kogo, K. Ishiguro, K. Tauchi, and R. Nomura.** 2001. Caveolin-2 is targeted to lipid droplets, a new "membrane domain" in the cell. J. Cell Biol. **152**:1079–1085.
12. **Gottwein, J. M., T. K. Scheel, B. Callendret, Y. P. Li, H. B. Eccleston, R. E. Engle, S. Govindarajan, W. Satterfield, R. H. Purcell, C. M. Walker, and J. Bukh.** Novel infectious cDNA clones of hepatitis C virus genotype 3a (strain S52) and 4a (strain ED43): genetic analyses and *in vivo* pathogenesis studies. J. Virol. **84**:5277–5293.
13. **Hammache, D., G. Pieroni, N. Yahi, O. Delezay, N. Koch, H. Lafont, C. Tamalet, and J. Fantini.** 1998. Specific interaction of HIV-1 and HIV-2 surface envelope glycoproteins with monolayers of galactosylceramide and ganglioside GM3. J. Biol. Chem. **273**:7967–7971.
14. **Hang, J. Q., Y. Yang, S. F. Harris, V. Leveque, H. J. Whittington, S. Rajyaguru, G. Ao-Ieong, M. F. McCown, A. Wong, A. M. Giannetti, S. Le Pogam, F. Talamas, N. Cammack, I. Najera, and K. Klumpp.** 2009. Slow binding inhibition and mechanism of resistance of non-nucleoside polymerase inhibitors of hepatitis C virus. J. Biol. Chem. **284**:15517–15529.
15. **Huang, H., F. Sun, D. M. Owen, W. Li, Y. Chen, M. Gale, Jr., and J. Ye.** 2007. Hepatitis C virus production by human hepatocytes dependent on assembly and secretion of very low-density lipoproteins. Proc. Natl. Acad. Sci. U. S. A. **104**:5848–5853.
16. **Ishii, N., K. Watashi, T. Hishiki, K. Goto, D. Inoue, M. Hijikata, T. Wakita, N. Kato, and K. Shimotohno.** 2006. Diverse effects of cyclosporine on hepatitis C virus strain replication. J. Virol. **80**:4510–4520.
17. **Kashiwagi, T., K. Hara, M. Kohara, K. Kohara, J. Iwahashi, N. Hamada, H. Yoshino, and T. Toyoda.** 2002. Kinetic analysis of C-terminally truncated RNA-dependent RNA polymerase of hepatitis C virus. Biochem. Biophys. Res. Commun. **290**:1188–1194.
18. **Kato, T., T. Date, M. Miyamoto, A. Furusaka, K. Tokushige, M. Mizokami, and T. Wakita.** 2003. Efficient replication of the genotype 2a hepatitis C virus subgenomic replicon. Gastroenterology **125**:1808–1817.
19. **Kiyosawa, K., T. Sodeyama, E. Tanaka, Y. Gibo, K. Yoshizawa, Y. Nakano, S. Furuta, Y. Akahane, K. Nishioka, R. H. Purcell, et al.** 1990. Interrelationship of blood transfusion, non-A, non-B hepatitis and hepatocellular carcinoma: analysis by detection of antibody to hepatitis C virus. Hepatology **12**:671–675.
20. **Lambot, M., S. Fretier, A. Op De Beeck, B. Quatannens, S. Lestavel, V. Clavey, and J. Dubuisson.** 2002. Reconstitution of hepatitis C virus envelope glycoproteins into liposomes as a surrogate model to study virus attachment. J. Biol. Chem. **277**:20625–20630.
21. **Lemon, S., C. Walker, M. Alter, and M. Yi.** 2007. Hepatitis C virus, p. 1253–1304. *In* D. M. Knipe, P. M. Howley, D. E. Griffin, R. A. Lamb, M. A. Martin, B. Roizman, and S. E. Straus (ed.), Fields virology, 5th ed. Lippincott Williams & Wilkins, Philadelphia, PA.
22. **Mahfoud, R., N. Garmy, M. Maresca, N. Yahi, A. Puigserver, and J. Fantini.** 2002. Identification of a common sphingolipid-binding domain in Alzheimer, prion, and HIV-1 proteins. J. Biol. Chem. **277**:11292–11296.
23. **Miyake, Y., Y. Kozutsumi, S. Nakamura, T. Fujita, and T. Kawasaki.** 1995. Serine palmitoyltransferase is the primary target of a sphingosine-like immunosuppressant, ISP-1/myriocin. Biochem. Biophys. Res. Commun. **211**: 396–403.
24. **Miyanari, Y., K. Atsuzawa, N. Usuda, K. Watashi, T. Hishiki, M. Zayas, R. Bartenschlager, T. Wakita, M. Hijikata, and K. Shimotohno.** 2007. The lipid droplet is an important organelle for hepatitis C virus production. Nat. Cell Biol. **9**:1089–1097.
25. **Murayama, A., T. Date, K. Morikawa, D. Akazawa, M. Miyamoto, M. Kaga, K. Ishii, T. Suzuki, T. Kato, M. Mizokami, and T. Wakita.** 2007. The NS3 helicase and NS5B-to-3′X regions are important for efficient hepatitis C virus strain JFH-1 replication in Huh7 cells. J. Virol. **81**:8030–8040.
26. **Murayama, A., L. Weng, T. Date, D. Akazawa, X. Tian, T. Suzuki, T. Kato, Y. Tanaka, M. Mizokami, T. Wakita, and T. Toyoda.** 2010. RNA polymerase activity and specific RNA structure are required for efficient HCV replication in cultured cells. PLoS Pathog. **6**:e1000885.
27. **Ostermeyer, A. G., J. M. Paci, Y. Zeng, D. M. Lublin, S. Munro, and D. A. Brown.** 2001. Accumulation of caveolin in the endoplasmic reticulum redirects the protein to lipid storage droplets. J. Cell Biol. **152**:1071–1078.
28. **Saito, I., T. Miyamura, A. Ohbayashi, H. Harada, T. Katayama, S. Kikuchi, Y. Watanabe, S. Koi, M. Onji, Y. Ohta, et al.** 1990. Hepatitis C virus infection is associated with the development of hepatocellular carcinoma. Proc. Natl. Acad. Sci. U. S. A. **87**:6547–6549.
29. **Sakamoto, H., K. Okamoto, M. Aoki, H. Kato, A. Katsume, A. Ohta, T. Tsukuda, N. Shimma, Y. Aoki, M. Arisawa, M. Kohara, and M. Sudoh.** 2005. Host sphingolipid biosynthesis as a target for hepatitis C virus therapy. Nat. Chem. Biol. **1**:333–337.
30. **Shi, S. T., K. J. Lee, H. Aizaki, S. B. Hwang, and M. M. Lai.** 2003. Hepatitis C virus RNA replication occurs on a detergent-resistant membrane that cofractionates with caveolin-2. J. Virol. **77**:4160–4168.
31. **Simister, P., M. Schmitt, M. Geitmann, O. Wicht, U. H. Danielson, R. Klein, S. Bressanelli, and V. Lohmann.** 2009. Structural and functional analysis of hepatitis C virus strain JFH1 polymerase. J. Virol. **83**:11926–11939.
32. **Tsukiyama-Kohara, K., S. Tone, I. Maruyama, K. Inoue, A. Katsume, H. Nuriya, H. Ohmori, J. Ohkawa, K. Taira, Y. Hoshikawa, F. Shibasaki, M. Reth, Y. Minatogawa, and M. Kohara.** 2004. Activation of the CKI-CDK-Rb-E2F pathway in full genome hepatitis C virus-expressing cells. J. Biol. Chem. **279**:14531–14541.
33. **Umehara, T., M. Sudoh, F. Yasui, C. Matsuda, Y. Hayashi, K. Chayama, and M. Kohara.** 2006. Serine palmitoyltransferase inhibitor suppresses HCV replication in a mouse model. Biochem. Biophys. Res. Commun. **346**:67–73.
34. **Wasley, A., and M. J. Alter.** 2000. Epidemiology of hepatitis C: geographic differences and temporal trends. Semin. Liver Dis. **20**:1–16.
35. **Watashi, K., N. Ishii, M. Hijikata, D. Inoue, T. Murata, Y. Miyanari, and K. Shimotohno.** 2005. Cyclophilin B is a functional regulator of hepatitis C virus RNA polymerase. Mol. Cell **19**:111–122.
36. **Weng, L., J. Du, J. Zhou, J. Ding, T. Wakita, M. Kohara, and T. Toyoda.** 2009. Modification of hepatitis C virus 1b RNA polymerase to make a highly active JFH1-type polymerase by mutation of the thumb domain. Arch. Virol. **154**:765–773.
37. **Yasuda, S., H. Kitagawa, M. Ueno, H. Ishitani, M. Fukasawa, M. Nishijima, S. Kobayashi, and K. Hanada.** 2001. A novel inhibitor of ceramide trafficking from the endoplasmic reticulum to the site of sphingomyelin synthesis. J. Biol. Chem. **276**:43994–44002.
38. **Zhong, J., P. Gastaminza, G. Cheng, S. Kapadia, T. Kato, D. R. Burton, S. F. Wieland, S. L. Uprichard, T. Wakita, and F. V. Chisari.** 2005. Robust hepatitis C virus infection in vitro. Proc. Natl. Acad. Sci. U. S. A. **102**:9294–9299.

blood

2010 116: 4926-4933
Prepublished online Aug 23, 2010;
doi:10.1182/blood-2010-05-283358

Persistent expression of the full genome of hepatitis C virus in B cells induces spontaneous development of B-cell lymphomas in vivo

Yuri Kasama, Satoshi Sekiguchi, Makoto Saito, Kousuke Tanaka, Masaaki Satoh, Kazuhiko Kuwahara, Nobuo Sakaguchi, Motohiro Takeya, Yoichi Hiasa, Michinori Kohara and Kyoko Tsukiyama-Kohara

Blood (print ISSN 0006-4971, online ISSN 1528-0020), is published weekly by the American Society of Hematology, 2021 L St, NW, Suite 900, Washington DC 20036.

Persistent expression of the full genome of hepatitis C virus in B cells induces spontaneous development of B-cell lymphomas in vivo

*Yuri Kasama,[1] *Satoshi Sekiguchi,[2] Makoto Saito,[1] Kousuke Tanaka,[1] Masaaki Satoh,[1] Kazuhiko Kuwahara,[3] Nobuo Sakaguchi,[3] Motohiro Takeya,[4] Yoichi Hiasa,[5] Michinori Kohara,[2] and Kyoko Tsukiyama-Kohara[1]

[1]Department of Experimental Phylaxiology, Faculty of Life Sciences, Kumamoto University, Kumamoto, Japan; [2]Department of Microbiology and Cell Biology, Tokyo Metropolitan Institute of Medical Science, Tokyo, Japan; [3]Department of Immunology, Faculty of Life Sciences, Kumamoto University, Kumamoto, Japan; [4]Department of Cell Pathology, Faculty of Life Sciences, Kumamoto University, Kumamoto, Japan; and [5]Department of Gastroenterology and Metabology, Ehime University Graduate School of Medicine, To-on, Ehime, Japan

Extrahepatic manifestations of hepatitis C virus (HCV) infection occur in 40%-70% of HCV-infected patients. B-cell non-Hodgkin lymphoma is a typical extrahepatic manifestation frequently associated with HCV infection. The mechanism by which HCV infection of B cells leads to lymphoma remains unclear. Here we established HCV transgenic mice that express the full HCV genome in B cells (RzCD19Cre mice) and observed a 25.0% incidence of diffuse large B-cell non-Hodgkin lymphomas (22.2% in males and 29.6% in females) within 600 days after birth. Expression levels of aspartate aminotransferase and alanine aminotransferase, as well as 32 different cytokines, chemokines and growth factors, were examined. The incidence of B-cell lymphoma was significantly correlated with only the level of soluble interleukin-2 receptor α subunit (sIL-2Rα) in RzCD19Cre mouse serum. All RzCD19Cre mice with substantially elevated serum sIL-2Rα levels (> 1000 pg/mL) developed B-cell lymphomas. Moreover, compared with tissues from control animals, the B-cell lymphoma tissues of RzCD19Cre mice expressed significantly higher levels of IL-2Rα. We show that the expression of HCV in B cells promotes non-Hodgkin–type diffuse B-cell lymphoma, and therefore, the RzCD19Cre mouse is a powerful model to study the mechanisms related to the development of HCV-associated B-cell lymphoma. (*Blood.* 2010;116(23):4926-4933)

Introduction

More than 175 million people worldwide are infected with hepatitis C virus (HCV), a positive-strand RNA virus that infects both hepatocytes and peripheral blood mononuclear cells.[1] Chronic HCV infection may lead to hepatitis, liver cirrhosis, hepatocellular carcinomas[2,3] and lymphoproliferative diseases such as B-cell non-Hodgkin lymphoma and mixed-cryoglobulinemia.[1,4-6] B-cell non-Hodgkin lymphoma is a typical extrahepatic manifestation frequently associated with HCV infection[7] with geographic and ethnic variability.[8,9] Based on a meta-analysis, the prevalence of HCV infection in patients with B-cell non-Hodgkin lymphoma is approximately 15%.[8] The HCV envelope protein E2 binds human CD81,[10] a tetraspanin expressed on various cell types including lymphocytes, and activates B-cell proliferation[11]; however, the precise mechanism of disease onset remains unclear. We previously developed a transgenic mouse model that conditionally expresses HCV cDNA (nucleotides 294-3435), including the viral genes that encode the core, E1, E2, and NS2 proteins, using the Cre/*lox*P system (in core~NS2 [CN2] mice).[12,13] The conditional transgene activation of the HCV cDNA (core, E1, E2, and NS2) protects mice from Fas-mediated lethal acute liver failure by inhibiting cytochrome c release from mitochondria.[13] In HCV-infected mice, persistent HCV protein expression is established by targeted disruption of *irf-1*, and high incidences of lymphoproliferative disorders are found in CN2 *irf-1*$^{-/-}$ mice.[14] Infection and replication of HCV also occur in B cells,[15,16] although the direct effects, particularly in vivo, of HCV infection on B cells have not been clarified.

To define the direct effect of HCV infection on B cells in vivo, we crossed transgenic mice with an integrated full-length HCV genome (Rz) under the conditional Cre/*lox*P expression system with mice expressing the Cre enzyme under transcriptional control of the B lineage–restricted gene *CD19*,[17] we addressed the effects of HCV transgene expression in this study.

Methods

Animal experiments

Wild-type (WT), Rz, CD19Cre, RzCD19Cre mice (129/sv, BALB/c, and C57BL/6J mixed background), and MxCre/CN2-29 mice (C57BL/6J background) were maintained in conventional animal housing under specific pathogen-free conditions. All animal experiments were performed according to the guidelines of the Tokyo Metropolitan Institute of Medical Science or the Kumamoto University Subcommittee for Laboratory Animal Care. The protocol was approved by the Institutional Review Boards of both facilities.

Measurements of HCV protein and RNA

Mice were anesthetized and bled, and tissues (spleen, lymph nodes, liver, and tumors) were homogenized in lysis buffer (1% sodium dodecyl sulfate; 0.5% (wt/vol) nonyl phenoxypolyethoxylethanol; 0.15M NaCl; 10 mM

Submitted May 2, 2010; accepted August 13, 2010. Prepublished online as *Blood* First Edition paper, August 23, 2010; DOI 10.1182/blood-2010-05-283358.

*Y.K. and S.S. contributed equally to this work.

The online version of this article contains a data supplement.

The publication costs of this article were defrayed in part by page charge payment. Therefore, and solely to indicate this fact, this article is hereby marked "advertisement" in accordance with 18 USC section 1734.

tris(hydroxymethyl)aminomethane, pH 7.4) using a Dounce homogenizer. The concentration of HCV core protein in tissue lysates was measured using an HCV antigen enzyme-linked immunosorbent assay (ELISA; Ortho).[18] HCV mRNA was isolated by a guanidine thiocyanate protocol using ISOGEN (Nippon Gene) and was detected by reverse transcription polymerase chain reaction (RT-PCR) amplification using primers specific for the 5′ untranslated region of the *HCR6* sequence.[19,20] Reverse transcription was performed using Superscript III reverse transcriptase (Invitrogen) with random primers. PCR primers NCR-F (5′-TTCACGCAGAAAGCGTCTAGCCAT-3′) and NCR-R (5′-TCGTCCTGGCAATTCCGGTGTACT-3′) were used for the first round of HCV cDNA amplification, and the resulting product was used as a template for a second round of amplification using primers NCR-F INNER (5′-TTCCGCAGACCACTATGGCT-3′) and NCR-R INNER (5′-TTCCGCAGACCACTATGGCT-3′).

Collection of serum for chemokine ELISA

Blood samples were collected from the supraorbital veins or by heart puncture of killed mice. Blood samples were centrifuged at 10 000*g* for 15 minutes at 4°C to isolate the serum.[21] Serum concentrations of interleukin (IL)–1α, IL-1β, IL-2, IL-3, IL-4, IL-5, IL-6, IL-9, IL-10, IL-12(p40), IL-12(p70), IL-13, IL-17, Eotaxin, granulocyte colony-stimulating factor (CSF), granulocyte–macrophage–CSF, interferon (IFN)–γ, keratinocyte-derived chemokine (KC), monocyte chemotactic protein-1, macrophage inflammatory protein (MIP)–1α, MIP-1β, Regulated upon Activation, Normal T-cell Expressed, and Secreted, tumor necrosis factor-α, IL-15, fibroblast growth factor-basic, leukemia inhibitory factor, macrophage-CSF, human monokine induced by gamma interferon, MIP-2, platelet-derived growth factorβ, and vascular endothelial growth factor were measured using the Bio-Plex Pro assay (Bio-Rad). Serum soluble IL-2 receptor α (sIL-2Rα) concentrations were determined by ELISA (DuoSet ELISA Development System; R&D Systems). Serum aspartate aminotransferase (AST) and alanine aminotransferase (ALT) activities were determined using a commercially available kit (Transaminase CII test; Wako Pure Chemical Industries).

Histology and immunohistochemical staining

Mouse tissues were fixed with 4% formaldehyde (Mildform 10 N; Wako Pure Chemical Industries), dehydrated with an ethanol series, embedded in paraffin, sectioned (10-μm thick) and stained with hematoxylin and eosin. For tissue immunostaining, paraffin was removed from the sections using xylene following the standard method,[14] and sections were incubated with anti-CD3 or anti-CD45R (Santa Cruz Biotechnology) in phosphate-buffered saline without Ca^{2+} and Mg^{2+} (pH 7.4) but with 5% skim milk. Next, the sections were incubated with biotinylated anti-rat immunoglobulin (Ig)G (1:500), followed by incubation with horseradish peroxidase-conjugated avidin-biotin complex (Dako Corp), and the color reaction was developed using 3,3′-diaminobenzidine. Sections were observed under an optical microscope (Carl Zeiss).

Detection of immunoglobulin gene rearrangements by PCR

Genomic DNA was isolated from tumor tissues, and PCR was performed as described.[22] In brief, PCR reaction conditions were 98°C for 3 minutes; 30 cycles at 98°C for 30 seconds, 60°C for 30 seconds, 72°C for 1.5 minutes, and 72°C for 10 minutes. Mouse Vk genes were amplified using previously described primers.[23] Amplification of mouse Vj genes was performed using Vκcon (5′-GGCTGCAGSTTCAGTGGCAGTGGRTCWGGRAC-3′; R, purine; W, A or T) and Jκ5 (5′-TGCCACGTCAACTGATAATGAGCCCTCTC-3′) as described.[24]

Results

Establishment of transgenic mice with B lineage–restricted HCV gene expression

We defined the direct effect of HCV infection on B cells in vivo by crossing transgenic mice that had an integrated full-length HCV genome (Rz) under the conditional Cre/*lox*P expression system (Figure 1A upper schematic)[12,19,25] with mice that expressed the Cre enzyme under transcriptional control of the B lineage–restricted gene *CD19*[17] (RzCD19Cre; Figure 1A lower schematic). Expression of the HCV transgene in RzCD19Cre mice was confirmed by ELISA (Figure 1B); a substantial level of HCV core protein was detected in the spleen (370.9 ± 10.2 pg/mg total protein), but levels were lower in the liver (0.32 ± 0.03 pg/mg) and plasma (not detectable). RT-PCR analysis of peripheral blood lymphocytes (PBLs) from RzCD19Cre mice indicated the presence of HCV transcripts (Figure 1C). The weights of RzCD19Cre, Rz (with the full HCV genome transgene alone), CD19Cre (with the Cre gene knock-in at the CD19 gene locus) and WT mice were measured weekly for more than 600 days post birth; there were no significant differences between these groups (data not shown; the total number of transgenic and WT mice was approximately 200). The survival rate in each group was also measured for > 600 days (Figure 1D); survival in the female RzCD19Cre group was lower than that of the other groups.

The spontaneous development of B-cell lymphomas in the RzCD19Cre mouse

At 600 days post birth, mice (n = 140) were killed by bleeding under anesthesia, and tissues (spleen, lymph node, liver, and tumors) were excised and examined by hematoxylin and eosin staining (Figure 2A; supplemental Figure 1, available on the *Blood* Web site; see the Supplemental Materials link at the top of the online article). The incidence of B-cell lymphoma in RzCD19Cre mice was 25.0% (22.2% in males and 29.6% in females) and was significantly higher than the incidence in the HCV-negative groups (Table 1). This incidence is significantly higher than those of the other cell-type tumors developed spontaneously in all mouse groups (supplemental Table 1). Because nodular proliferation of CD45R-positive atypical lymphocytes was observed, lymphomas were diagnosed as typical diffuse B-cell non-Hodgkin lymphomas (Figure 2Aiv,vi-vii; supplemental Figure 1B,E,H,M). Mitotic cells were also positive for CD45R (Figure 2Avi arrowheads). CD3-positive T-lymphocytes were small and had a scattered distribution. Intrahepatic lymphomas had the same immunophenotypic characteristics as B-cell lymphomas (supplemental Figure 1K arrowheads, inset; 1L–N, ID No. 24-4, RzCD19Cre mouse); lymphoma tissues were markedly different compared with the control lymph node (Figure 2Ai,iii,v; ID No. 47-4, CD19Cre mouse) and liver (supplemental Figure 1J; ID No. 24-2, Rz mouse; tissues were from a littermate of the mice used to generate the data in supplemental Figure 1D-I,K-N). All samples were reviewed by at least 2 expert pathologists and classified according to World Health Organization classification.[26] Lymphomas were mostly CD45R positive and located in the mesenteric lymph nodes (Figure 2A; supplemental Figure 1), and some were identified as intrahepatic lymphomas (incidence, 4.2%; supplemental Figure 1K-N). HCV gene expression was detected in all B-cell lymphomas of RzCD19Cre mice (Figure 2B).

To examine the Ig gene configuration in the B-cell lymphomas of the RzCD19Cre mice, genomic DNA was isolated and analyzed by PCR. Ig gene rearrangements were identified in each case (Figure 2C). Genomic DNA isolated from the tumors of a germinal center–associated nuclear protein (GANP) transgenic mouse (GANP Tg#3) yielded a predominant Jk5 PCR product (Figure 2C, Vκ-Jκ); a predominant JH1 product and a minor JH2 product (supplemental Figure 2, DH-JH) were also identified, as previously reported,[22] indicating that the lymphoma cells proliferated from the transformation of an oligo B-cell clone. The B-cell lymphomas of

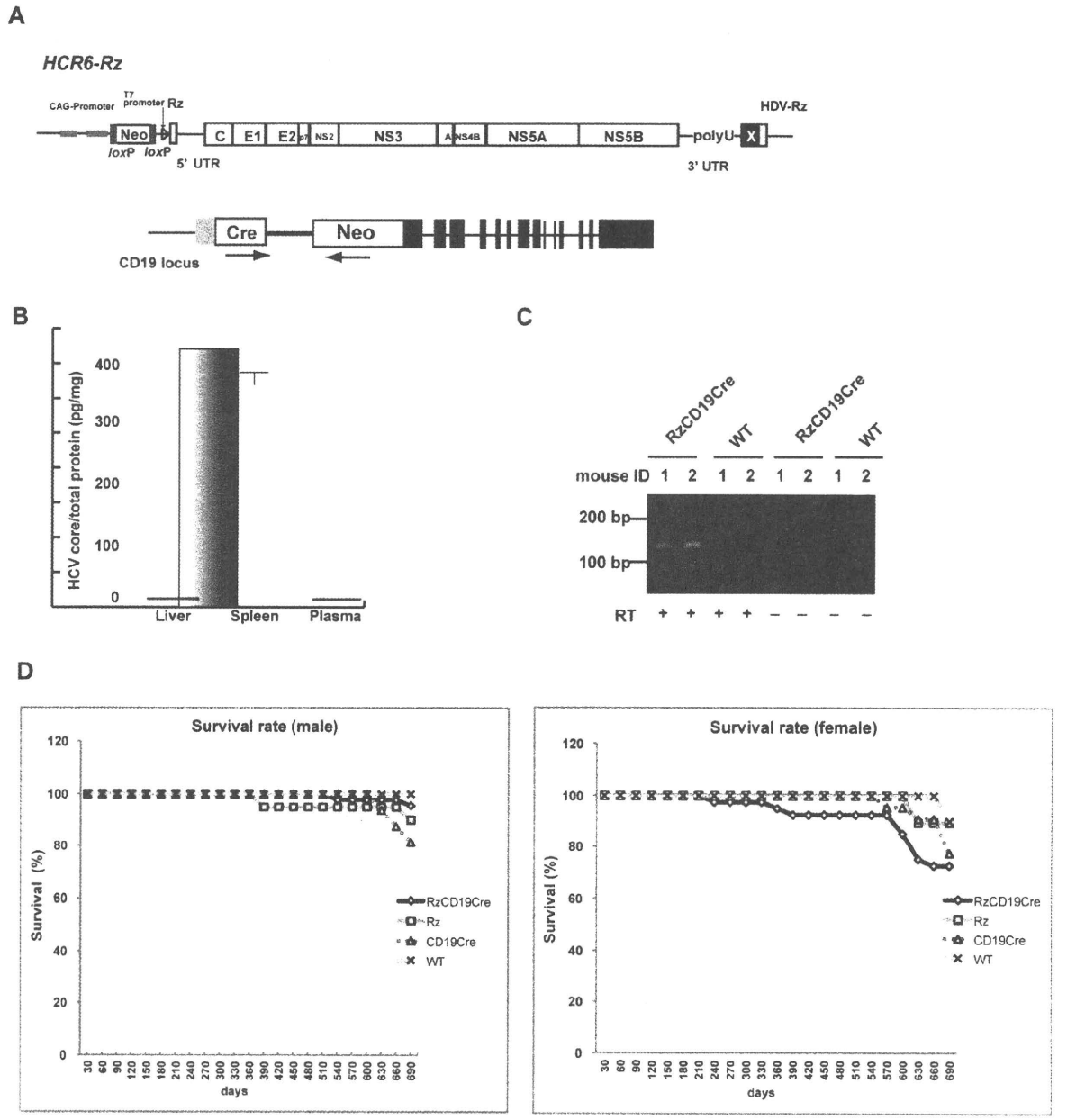

Figure 1. Establishment of RzCD19Cre mice. (A) Schematic diagram of the transgene structure comprising the complete HCV genome (*HCR6-Rz*). HCV genome expression was regulated by the Cre/*loxP* expression cassette (top diagram). The Cre transgene was located in the CD19 locus (bottom diagram). (B) Expression of HCV core protein in the liver, spleen, and plasma of RzCD19Cre mice was quantified by core ELISA. Data represent the mean ± SD (n = 3). (C) Detection of HCV RNA in PBLs by RT-PCR. Samples that included the RT reaction are indicated by +, and those that did not include the RT reaction are indicated by –. (D) Survival rates of male and female RzCD19Cre mice (males, n = 45; females, n = 40), Rz mice (males, n = 20; females, n = 19), CD19Cre mice (males, n = 16; females, n = 22), and WT mice (males, n = 5; females, n = 10).

8 RzCD19Cre mice (mouse ID Nos. 24-1, 54-1, 56-5, 69-5, 42-4, 43-4, 36-3 [data not shown] and 62-2 [data not shown]) yielded a Jκ-5 gene amplification product, and the lymphomas from 3 other mice had the alternative gene configurations Jκ-1 (mouse ID No. 31-4), Jκ-2 (mouse ID No. 24-4) and Jκ-3 (mouse ID No. 42-4; Figure 2C). PCR amplification products from the genes JH4 (mouse ID Nos. 24-1, 24-4, 54-1, 43-4, 56-5, 69-5, 62-2 [data not shown], 36-3 [data not shown]), JH1 (mouse ID Nos. 31-4, 42-4) and JH3 (mouse ID Nos. 31-4, 42-4, 56-5, 43-4, 36-3 [data not shown]) were also detected (supplemental Figure 2). The mutation frequencies in the Jκ-1, -3 and -5 genes were the same as the mutation frequency in the genomic V-region gene.[22] Few or no sequence differences in the variable region were identified among clones from which DNA was amplified. These results indicate the possibility that tumors judged as B-cell lymphomas based on pathology criteria were derived from the transformation of a single germinal center of B-cell origin.

To rule out the oncogenic effect caused by a transgenic integration into a specific genomic locus, we examined if HCV transgene inserted into another genomic site also causes B-cell lymphomas using another HCV transgenic mouse strain, MxCre/CN2-29 (supplemental Figure 3). Expression of the HCV CN2

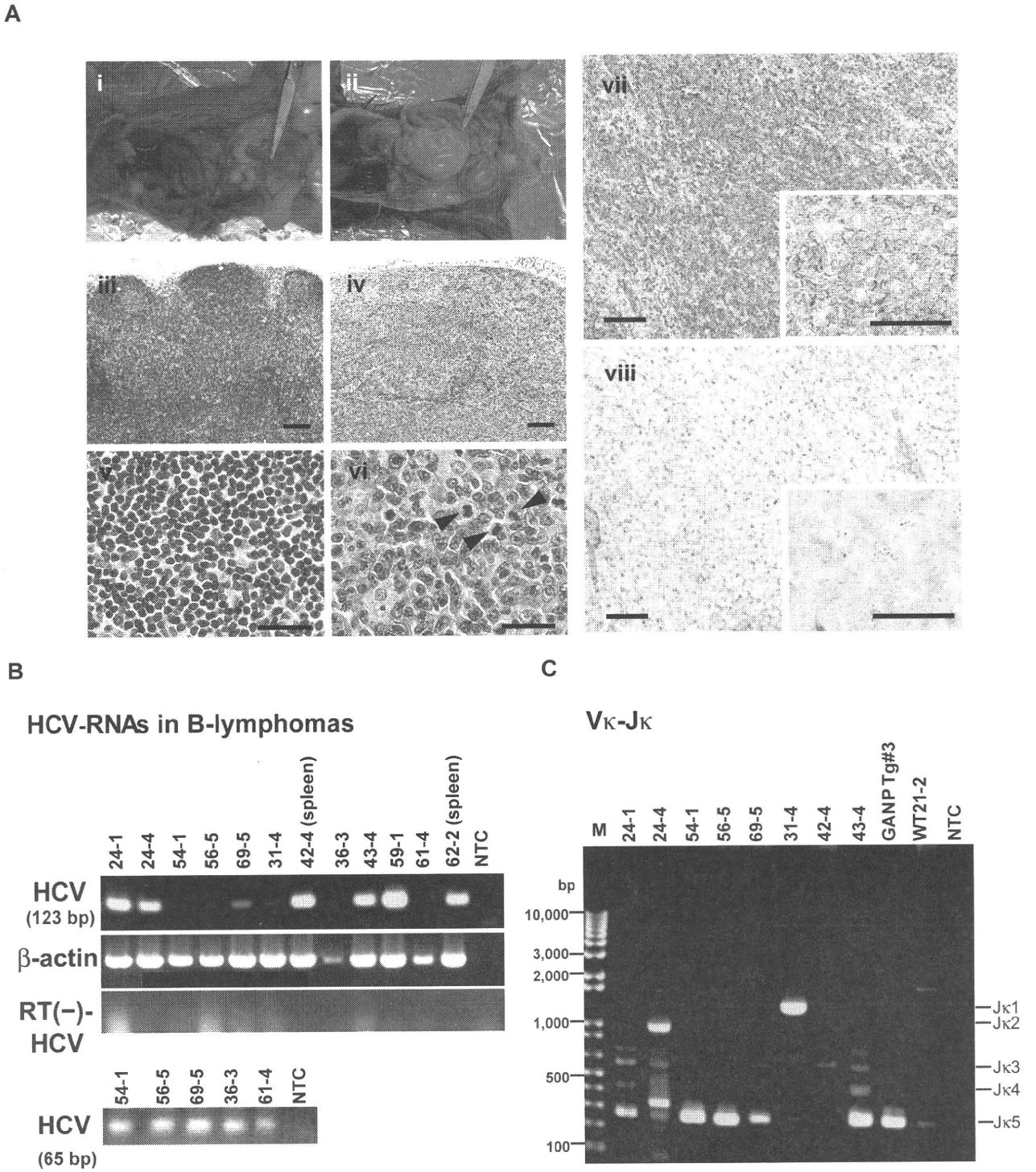

Figure 2. Histopathologic analysis of B-cell lymphomas in RzCD19Cre mouse tissues. (A) Histologic analysis of tissues from a normal mouse (i, iii, v; CD19Cre mouse, ID No. 47-4, male) and a B-cell lymphoma from a RzCD19Cre mouse (ii, iv, vi; ID No. 69-5, male). Paraformaldehyde-fixed and paraffin-embedded tumor tissues were stained with hematoxylin and eosin (iii-vi) or immunostained using anti-CD45R (vii; bottom right, inset) and anti-CD3 (viii; bottom right, inset). Also shown is a macroscopic view of the lymphoma from a mesenchymal lymph node (ii, indicated by forceps), which is not visible in the normal mouse (i). Mitotic cells are indicated with arrowheads (vi). Scale bars: 100 μm (iii-iv, vii-viii) and 20 μm (v-vi, insets in vii-viii). (B) Expression of HCV RNA in B-cell lymphomas from RzCD19Cre mice was examined by RT-PCR. The first round of PCR amplification yielded a 123-base pair fragment of HCV cDNA (upper panel), and a second round of PCR amplification yielded a 65-base pair fragment (lower panel). The β-actin mRNA was a control. As an additional control, the first and second rounds of amplification were performed using samples that had not been subjected to reverse transcription. NTC, no-template control. (C) Ig gene rearrangements in the tumors of RzCD19Cre mice. Genomic DNA isolated from B-cell lymphoma tissues of RzCD19Cre mice (ID Nos. 24-1, 24-4, 54-1, 56-5, 69-5, 31-4, 42-4, 43-4) and spleen tissues of a WT mouse (ID No. 21-2) was PCR amplified using primers specific for Vκ-Jκ genes. Amplification of controls was performed using genomic DNA isolated from a GANP transgenic mouse (GANP Tg#3) and in the absence of template DNA (no-template control, NTC). M, DNA ladder marker.

gene (nucleotides 294-3435)[12] was induced by the Mx promoter-driven cre recombinase with poly(I:C) induction[14] (supplemental Figure 3A). HCV core proteins were detected in both normal spleen (mouse ID Nos. 2, 3, 4) and intra-splenic B-cell lymphoma tissues

Table 1. Lymphoma incidence in HCV-expressing and control mice

HCV expression	Mouse genotype	No.	Incident B lymphoma, number (%)	Incident T lymphoma, number (%)
+	RzCD19Cre	72	18 (25.0)	3 (4.1)
−	Rz	34	1 (2.9)	1 (2.9)
−	CD19Cre	22	2 (9.1)	1 (4.5)
−	WT	12	1 (8.3)	1 (8.3)

(mouse ID Nos. 5, 6, 7) of MxCre/CN2-29 mice but not in spleens of the CN2-29 mouse (mouse ID No. 1, Figure 3B). After 12 months, the MxCre/CN2-29 mice developed B-cell lymphomas in the spleen at a high incidence (33.3%: 3/9), whereas the CN2-29 mice did not (0/13; supplemental Figure 3C), indicating that the development of B-cell lymphomas in HCV transgenic mice occurred similarly to RzCD19Cre mice. MxCre/CN2-29 mice also developed hepatocellular carcinomas (10%, 360 days, 17%, 480 days, 50%, 600 days after onset of HCV expression; Sekiguchi et al, submitted).

The results obtained in 2 HCV transgenic mouse strains indicate that the expression of the HCV gene or the proteins indeed induces the spontaneous development of B-cell lymphomas irrespective of the integrated site in the mouse genome.

The levels of cytokines and chemokines in B-cell lymphomas and other tumors and in tumor-free control mice

Abnormal induction of cytokine production occurs in HCV-associated non-Hodgkin lymphomas[27,28] and in patients with

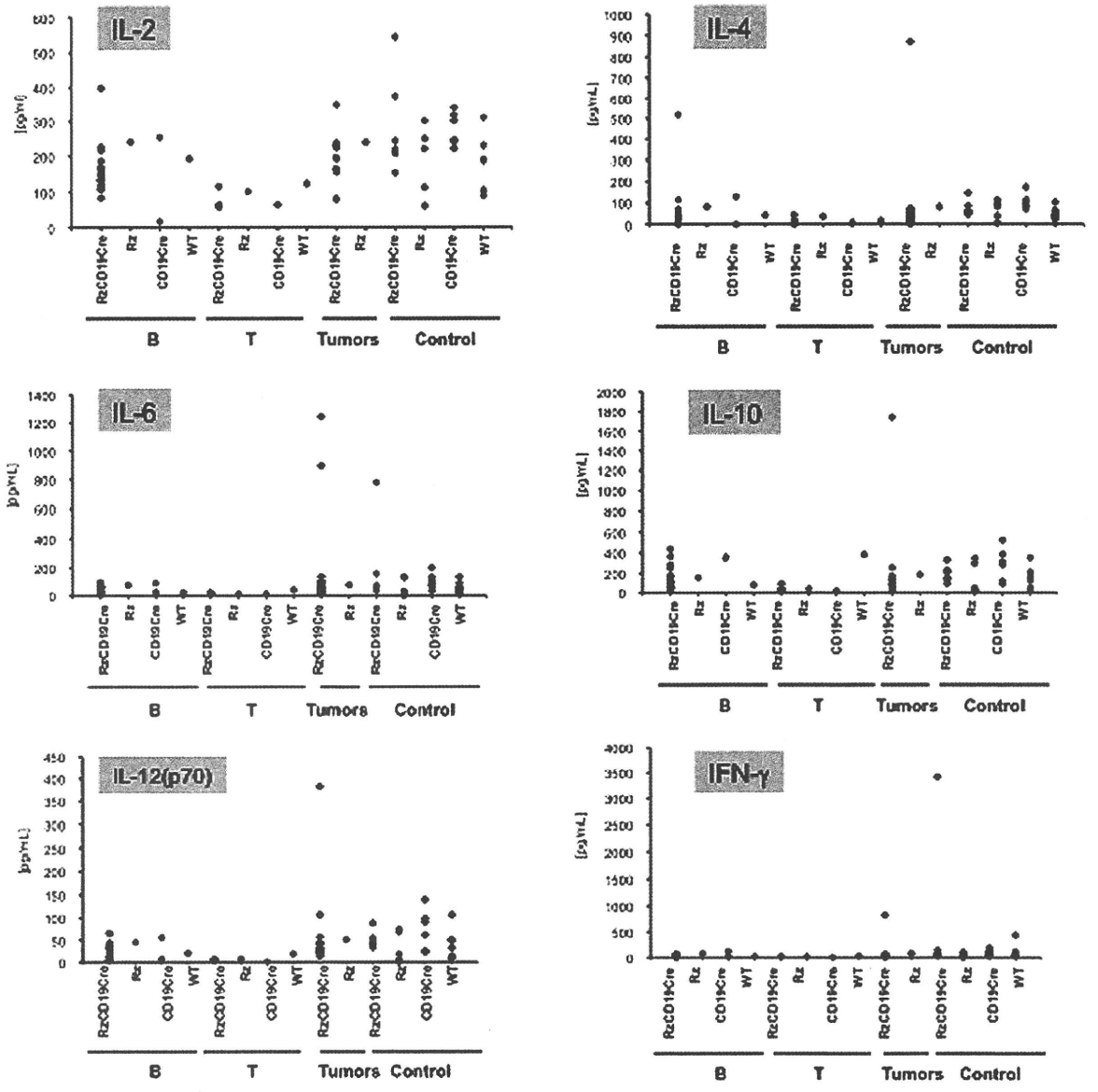

Figure 3. Analysis of serum cytokine levels using a multisuspension array system. The serum concentration levels of IL-2, IL-4, IL-6, IL-10, IL-12(p70), and IFN-γ were measured in RzCD19Cre mice with B-cell lymphomas (B), T-cell lymphomas (T), and other tumors (mammary tumor, sarcoma, and hepatocellular carcinoma) and in tumor-free RzCD19Cre, Rz, CD19Cr,e and WT mice.

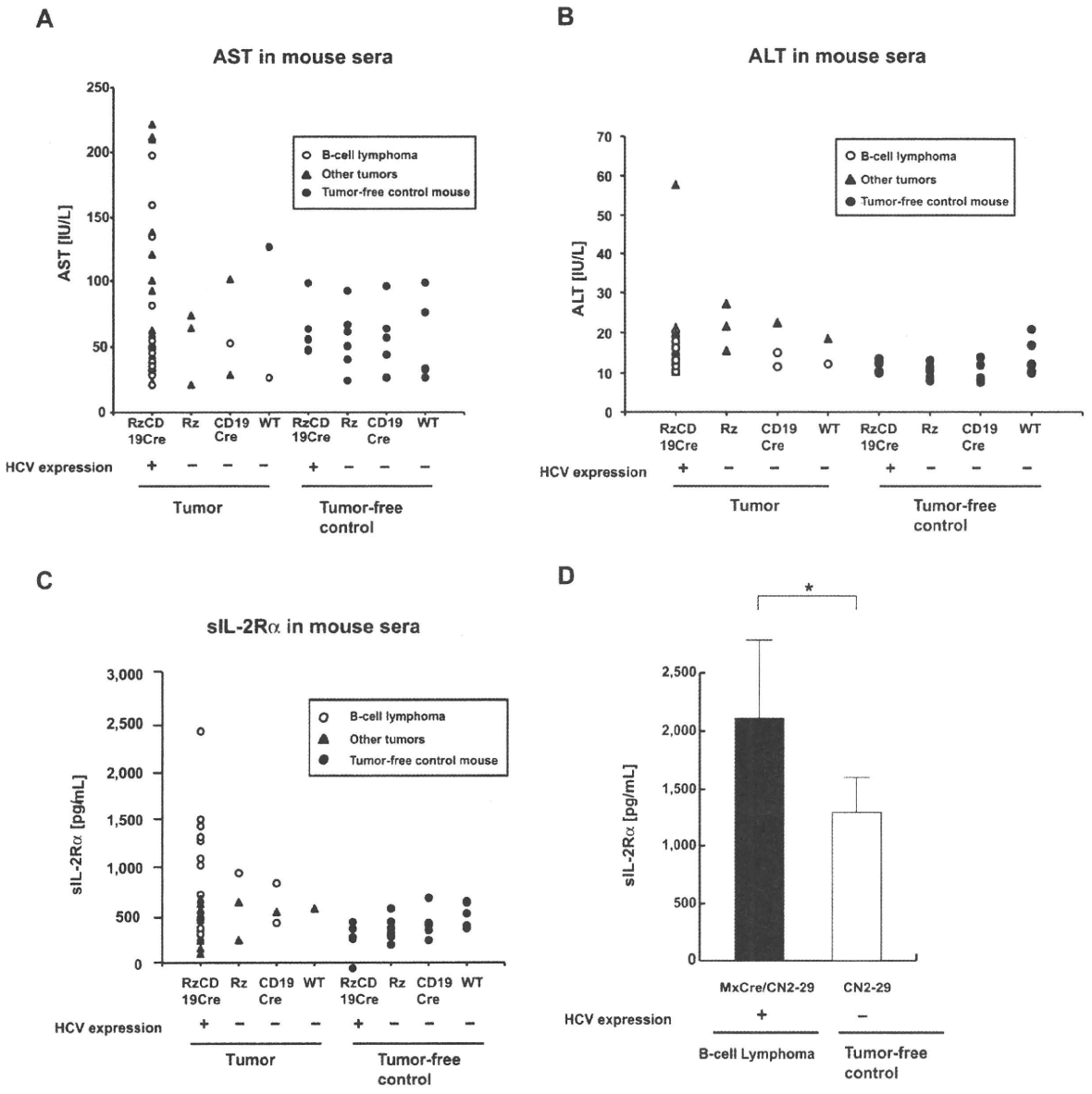

Figure 4. Serum titers of AST, ALT and soluble IL-2Rα in transgenic and control mice lacking or harboring B-cell lymphomas. (A-B) The AST (A) and ALT (B) assays were performed on serum samples from tumor-free control mice and the RzCD19Cre, Rz, CD19Cre and WT mice with or without B-cell lymphomas or other tumors. (C) ELISA analysis was performed to determine the sIL-2Rα concentration in serum samples from tumor-free control mice and the RzCD19Cre, Rz, CD19Cre, and WT mice with or without B-cell lymphomas or other tumors. (D) Concentration of soluble IL-2Rα in sera from transgenic (MxCre/CN2-29 or CN2-29) mice with or without B-cell lymphomas (*$P < .05$).

chronic hepatitis.[29,30] Therefore, we examined tumor cytokine and chemokine levels using a multisuspension array system. The levels of IL-2, IL-4, IL-6, IL-10, IL-12(p70), and IFN-γ (Figure 3), which may have a link with lymphoproliferation[14] or lymphoma[28,31] induced by HCV, and IL-1α, IL-1β, IL-3, IL-5, IL-9, IL-12(p40), IL-13, IL-17, Eotaxin, granulocyte-CSF, granulocyte–macrophage–CSF, KC, monocyte chemotactic protein-1, MIP-1α, MIP-1β, Regulated upon Activation, Normal T-cell Expressed, and Secreted, tumor necrosis factor-α, IL-15, fibroblast growth factor-basic, leukemia inhibitory factor, macrophage-CSF, human monokine induced by gamma interferon, MIP-2, platelet-derived growth factorβ and vascular endothelial growth factor (supplemental Figure 4) were measured in sera from mice with B-cell lymphomas, T-cell lymphomas, and other tumors and in sera from tumor-free RzCD19Cre, Rz, CD19Cre, and WT control mice. The levels of these cytokines and chemokines in sera from tumor-bearing RzCD19Cre mice with B-cell lymphomas were not significantly different from those of the control groups, and thus, changes in the expression of these cytokines and chemokines were not strictly correlated with the occurrence of B-cell lymphoma in RzCD19Cre mice.

The levels of amino transferases and sIL-2Rα in mice lacking or harboring B-cell lymphomas

We also examined the levels of AST and ALT in the RzCD19Cre, Rz, CD19Cre, and WT mice. There were no significant differences in the levels of AST and ALT in the sera of mice lacking or harboring B-cell lymphomas ($P > .05$; Figure 4A-B; AST:

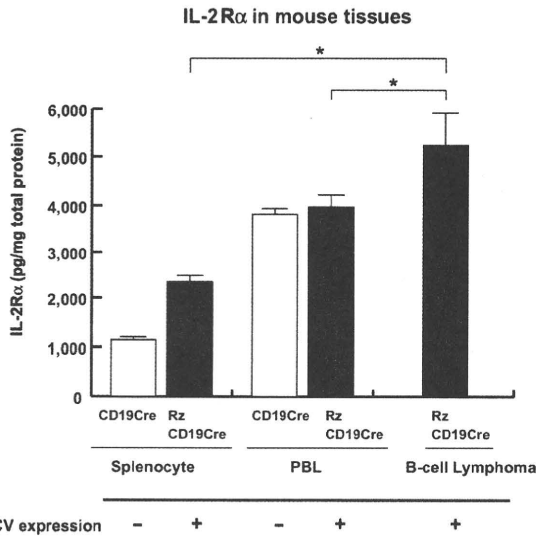

Figure 5. Levels of IL-2Rα in transgenic and control mice lacking or harboring B-cell lymphomas. The expression level of IL-2Rα in splenocytes and PBLs from CD19Cre and RzCD19Cre mice and in B-cell lymphomas from RzCD19Cre mice was measured by ELISA. IL-2Rα levels per total protein are indicated (picograms per milligram). Data from quadruplicate samples are shown as the mean ± SD (*$P < .05$).

RzCD19Cre mice with B-cell lymphomas, 72.2 ± 60.5 IU/L; normal controls, 55.2 ± 23.0 IU/L and ALT: RzCD19Cre mice with B-cell lymphomas, 14.2 ± 3.1 IU/L; normal controls, 11.5 ± 3.0 IU/L).

Finally, we examined the level of sIL-2Rα in the sera of the RzCD19Cre mice with B-cell lymphomas; sIL-2Rα is generated by proteolytic cleavage of IL-2Rα (CD25) residing on the surface of activated T and natural killer cells, monocytes, and certain tumor cells.[24,32] The average sIL-2Rα level in the RzCD19Cre mice with B-cell lymphomas (830.3 ± 533.0 pg/mL) was significantly higher than that in the tumor-free control groups, including the RzCD19Cre, Rz, CD19Cre and WT mice (499.9 ± 110.2 pg/mL; $P < .0057$; Figure 4C). The average sIL-2Rα levels in other tumor-containing groups (430.46 ± 141.15 pg/mL) were not significantly different from those in the tumor-free control groups ($P > .05$; Figure 4C). Moreover, all RzCD19Cre mice with a relatively high level of sIL-2Rα (> 1000 pg/mL) presented with B-cell lymphomas (Figure 4C).

We also examined the level of sIL-2Rα in MxCre/CN2-29 mice and observed a significant increase in sIL-2Rα in mice that expressed HCV and that had B-cell lymphomas compared with tumor-free control (CN2-29) mice (Figure 4D).

Expression of IL-2Rα in B-cell lymphomas of the RzCD19Cre mice

To examine whether sIL-2Rα was derived from lymphoma tissues, we quantified IL-2Rα concentrations in splenocytes, PBLs and B-cell lymphoma tissues (Figure 5). The concentration of IL-2Rα was significantly higher in splenocytes from RzCD19Cre mice compared with those from CD19Cre mice; the concentration was even higher in B-cell lymphoma tissues than in splenocytes from RzCD19Cre mice (Figure 5). These results strongly suggest that B-cell lymphomas directly contribute to the elevated serum concentrations of sIL-2Rα in RzCD19Cre mice.

Discussion

We have established HCV transgenic mice that have a high incidence of spontaneous B-cell lymphomas. In this animal model, the HCV transgene is expressed during the embryonic stage, and these RzCD19Cre mice are expected to be immunotolerant to the HCV transgene product. Thus, the results from this study reveal the potential for the HCV gene to induce B-cell lymphomas without inducing host immune responses against the HCV gene product. A retrospective study indicated that viral elimination reduced the incidence of malignant lymphoma in patients infected with HCV.[33] The results in our study may be consistent with this retrospective observation, indicating the significance of the direct effect of HCV infection on B-cell lymphoma development. Another HCV transgenic mouse strain (MxCre/CN2-29) showed the similarly high incidence of B-cell lymphoma, which strongly supported that development of B-cell lymphomas occurred by the expression of HCV transgene.

Recent findings have revealed the significance of B lymphocytes in HCV infection of liver-derived hepatoma cells.[34] In 4.2% of the RzCD19Cre mice, CD45R-positive intrahepatic lymphomas were identified, and infiltration of B cells into the hepatocytes was frequently observed (data not shown). These phenomena suggest that HCV could modify the in vivo tropism of B cells. The RzCD19Cre mouse is a powerful model system to address these mechanisms in vivo.

As a circulating membrane receptor, sIL-2Rα is localized in lymphoid cells and some other types of cancer cells and is highly expressed in several cancers[35-40] and autoimmune diseases.[41] Recent findings indicate a link between sIL-2Rα levels and hepatocellular carcinoma in Egyptian patients.[42] Appearing on the surface of leukemic cells derived from B and pre-B lymphocytes and other leukemic cells, IL-2Rα is one of the subunits of the IL-2 receptor, which is composed of an α chain (CD25), a β chain (CD122), and a γ chain (CD132).[43] IL-2R ectodomains are thought to be proteolytically cleaved from the cell surface[34,44,45] instead of produced as a result of posttranscriptional splicing.[24] In RzCD19Cre splenocytes, the level of IL-2Rα was higher than that in splenocytes from CD19Cre mice; however, serum concentrations of sIL-2Rα in RzCD19Cre mice without B-cell lymphomas did not show significant differences compared with other control groups (Rz, CD19Cre, and WT). These results indicate the possibility that HCV may increase IL-2Rα expression on B-cells; proteolytic cleavage of IL-2Rα was increased after B-cell lymphoma development in the RzCD19Cre mouse. The detailed mechanism that induces IL-2Rα as a result of HCV expression is still unclear at present, but we have found previously that the HCV core protein induces IL-10 expression in mouse splenocytes.[14] IL-10 up-regulates the expression of IL-2Rα (Tac/CD25) on normal and leukemic B lymphocytes,[46] and therefore, through IL-10, the HCV core protein might induce IL-2Rα in B cells of the RzCD19Cre mouse.

In conclusion, this study established an animal model that will likely provide critical information for the elucidation of molecular mechanism(s) underlying the spontaneous development of B-cell non-Hodgkin lymphoma after HCV infection. This knowledge should lead to therapeutic strategies to prevent the onset and/or progression of B-cell lymphomas.

Acknowledgments

We thank Dr T. Ito for assistance with pathology characterization and Dr T. Munakata for valuable comments.

This work was supported by grants from the Ministry of Health and Welfare of Japan and the Cooperative Research Project on Clinical and Epidemiologic Studies of Emerging and Re-emerging Infectious Diseases.

Authorship

Contribution: K.T.-K. conceived of the project; K.K., M.K., and K.T.-K. designed the studies; Y.K., S.S., M. Saito, K.T., M. Satoh, M.T., and K.T.-K. performed experiments and analyses; N.S. and Y.H. provided scientific advice; and K.T.-K. wrote the manuscript.

Conflict-of-interest disclosure: The authors declare no competing financial interests.

Correspondence: Kyoko Tsukiyama-Kohara, Department of Experimental Phylaxiology, Faculty of Life Sciences, Kumamoto University, Kumamoto 860-8556, Japan; e-mail: kkohara@kumamoto-u.ac.jp.

References

1. Ferri C, Monti M, La Civita L, et al. Infection of peripheral blood mononuclear cells by hepatitis C virus in mixed cryoglobulinemia. *Blood.* 1993; 82(12):3701-3704.
2. Saito I, Miyamura T, Ohbayashi A, et al. Hepatitis C virus infection is associated with the development of hepatocellular carcinoma. *Proc Natl Acad Sci U S A.* 1990;87(17):6547-6549.
3. Simonetti RG, Camma C, Fiorello F, et al. Hepatitis C virus infection as a risk factor for hepatocellular carcinoma in patients with cirrhosis. A case-control study. *Ann Intern Med.* 1992;116(2):97-102.
4. Silvestri F, Pipan C, Barillari G, et al. Prevalence of hepatitis C virus infection in patients with lymphoproliferative disorders. *Blood.* 1996;87(10): 4296-4301.
5. Ascoli V, Lo Coco F, Artini M, Levrero M, Martelli M, Negro F. Extranodal lymphomas associated with hepatitis C virus infection. *Am J Clin Pathol.* 1998;109(5):600-609.
6. Mele A, Pulsoni A, Bianco E, et al. Hepatitis C virus and B-cell non-Hodgkin lymphomas: an Italian multicenter case-control study. *Blood.* 2003; 102(3):996-999.
7. Dammacco F, Sansonno D, Piccoli C, Racanelli V, D'Amore FP, Lauletta G. The lymphoid system in hepatitis C virus infection: autoimmunity, mixed cryoglobulinemia, and overt B-cell malignancy. *Semin Liver Dis.* 2000;20(2):143-157.
8. Gisbert JP, Garcia-Buey L, Pajares JM, Moreno-Otero R. Prevalence of hepatitis C virus infection in B-cell non-Hodgkin's lymphoma: systematic review and meta-analysis. *Gastroenterology.* 2003;125(6):1723-1732.
9. Negri E, Little D, Boiocchi M, La Vecchia C, Franceschi S. B-cell non-Hodgkin's lymphoma and hepatitis C virus infection: a systematic review. *Int J Cancer.* 2004;111(1):1-8.
10. Pileri P, Uematsu Y, Campagnoli S, et al. Binding of hepatitis C virus to CD81. *Science.* 1998; 282(5390):938-941.
11. Rosa D, Saletti G, De Gregorio E, et al. Activation of naive B lymphocytes via CD81, a pathogenetic mechanism for hepatitis C virus-associated B lymphocyte disorders. *Proc Natl Acad Sci U S A.* 2005;102(51):18544-18549.
12. Wakita T, Taya C, Katsume A, et al. Efficient conditional transgene expression in hepatitis C virus cDNA transgenic mice mediated by the Cre/loxP system. *J Biol Chem.* 1998;273(15):9001-9006.
13. Machida K, Tsukiyama-Kohara K, Seike E, et al. Inhibition of cytochrome c release in Fas-mediated signaling pathway in transgenic mice induced to express hepatitis C viral proteins. *J Biol Chem.* 2001;276(15):12140-12146.
14. Machida K, Tsukiyama-Kohara K, Sekiguch S, et al. Hepatitis C virus and disrupted interferon signaling promote lymphoproliferation via type II CD95 and interleukins. *Gastroenterology.* 2009; 137(1):285-296,296 e281-211.
15. Lerat H, Rumin S, Habersetzer F, et al. In vivo tropism of hepatitis C virus genomic sequences in hematopoietic cells: influence of viral load, viral genotype, and cell phenotype. *Blood.* 1998; 91(10):3841-3849.
16. Karavattathayyil SJ, Kalkeri G, Liu HJ, et al. Detection of hepatitis C virus RNA sequences in B-cell non-Hodgkin lymphoma. *Am J Clin Pathol.* 2000;113(3):391-398.
17. Rickert RC, Roes J, Rajewsky K. B lymphocyte-specific, Cre-mediated mutagenesis in mice. *Nucleic Acids Res.* 1997;25(6):1317-1318.
18. Tanaka T, Lau JY, Mizokami M, et al. Simple fluorescent enzyme immunoassay for detection and quantification of hepatitis C viremia. *J Hepatol.* 1995;23(6):742-745.
19. Tsukiyama-Kohara K, Tone S, Maruyama I, et al. Activation of the CKI-CDK-Rb-E2F pathway in full genome hepatitis C virus-expressing cells. *J Biol Chem.* 2004;279(15):14531-14541.
20. Nishimura T, Kohara M, Izumi K, et al. Hepatitis C virus impairs p53 via persistent overexpression of 3beta-hydroxysterol Delta24-reductase. *J Biol Chem.* 2009;284(52):36442-36452.
21. Tsukiyama-Kohara K, Poulin F, Kohara M, et al. Adipose tissue reduction in mice lacking the translational inhibitor 4E-BP1. *Nat Med.* 2001; 7(10):1128-1132.
22. Fujimura S, Xing Y, Takeya M, et al. Increased expression of germinal center-associated nuclear protein RNA-primase is associated with lymphomagenesis. *Cancer Res.* 2005;65(13):5925-5934.
23. Miyazaki T, Kato I, Takeshita S, Karasuyama H, Kudo A. Lambda5 is required for rearrangement of the Ig kappa light chain gene in pro-B cell lines. *Int Immunol.* 1999;11(8):1195-1202.
24. Rubin LA, Galli F, Greene WC, Nelson DL, Jay G. The molecular basis for the generation of the human soluble interleukin 2 receptor. *Cytokine.* 1990;2(5):330-336.
25. Tsukiyama-Kohara K, Iizuka N, Kohara M, Nomoto A. Internal ribosome entry site within hepatitis C virus RNA. *J Virol.* 1992;66(3):1476-1483.
26. Jaffe ES, Harris NL, Stein H, Isaacson PG. Classification of lymphoid neoplasms: the microscope as a tool for disease discovery. *Blood.* 2008; 112(12):4384-4399.
27. el-Din HM, Attia MA, Hamza MR, Khaled HM, Thoraya MA, Eisa SA. Hepatitis C Virus and related changes in immunologic parameters in non Hodgkin's lymphoma patients. *Egypt J Immunol.* 2004;11(1):55-64.
28. Feldmann G, Nischalke HD, Nattermann J, et al. Induction of interleukin-6 by hepatitis C virus core protein in hepatitis C-associated mixed cryoglobulinemia and B-cell non-Hodgkin's lymphoma. *Clin Cancer Res.* 2006;12(15):4491-4498.
29. Mizuochi T, Ito M, Takai K, Yamaguchi K. Differential susceptibility of peripheral blood CD5+ and CD5− B cells to apoptosis in chronic hepatitis C patients. *Biochem Biophys Res Commun.* 2009; 389(3):512-515.
30. Bansal AS, Bruce J, Hogan PG, Prichard P, Powell EE. Serum soluble CD23 but not IL8, IL10, GM-CSF, or IFN-gamma is elevated in patients with hepatitis C infection. *Clin Immunol Immunopathol.* 1997;84(2):139-144.
31. Barrett L, Gallant M, Howley C, et al. Enhanced IL-10 production in response to hepatitis C virus proteins by peripheral blood mononuclear cells from human immunodeficiency virus-monoinfected individuals. *BMC Immunol.* 2008;9:28.
32. Rubin LA, Kurman CC, Fritz ME, et al. Soluble interleukin 2 receptors are released from activated human lymphoid cells in vitro. *J Immunol.* 1985;135(5):3172-3177.
33. Kawamura Y, Ikeda K, Arase Y, et al. Viral elimination reduces incidence of malignant lymphoma in patients with hepatitis C. *Am J Med.* 2007; 120(12):1034-1041.
34. Stamataki Z, Shannon-Lowe C, Shaw J, et al. Hepatitis C virus association with peripheral blood B lymphocytes potentiates viral infection of liver-derived hepatoma cells. *Blood.* 2009;113(3): 585-593.
35. Wasik MA, Sioutos N, Tuttle M, Butmarc JR, Kaplan WD, Kadin ME. Constitutive secretion of soluble interleukin-2 receptor by human T cell lymphoma xenografted into SCID mice. Correlation of tumor volume with concentration of tumor-derived soluble interleukin-2 receptor in body fluids of the host mice. *Am J Pathol.* 1994;144(5): 1089-1097.
36. Tsai MH, Chiou SH, Chow KC. Effect of platelet activating factor and butyrate on the expression of interleukin-2 receptor alpha in nasopharyngeal carcinoma cells. *Int J Oncol.* 2001;19(5):1049-1055.
37. Yano T, Yoshino I, Yokoyama H, et al. The clinical significance of serum soluble interleukin-2 receptors in lung cancer. *Lung Cancer.* 1996;15(1):79-84.
38. Tesarova P, Kvasnicka J, Umlaufova A, Homolkova H, Jirsa M, Tesar V. Soluble TNF and IL-2 receptors in patients with breast cancer. *Med Sci Monit.* 2000;6(4):661-667.
39. Maccio A, Lai P, Santona MC, Pagliara L, Melis GB, Mantovani G. High serum levels of soluble IL-2 receptor, cytokines, and C reactive protein correlate with impairment of T cell response in patients with advanced epithelial ovarian cancer. *Gynecol Oncol.* 1998;69(3):248-252.
40. Matsumoto T, Furukawa A, Sumiyoshi Y, Akiyama KY, Kanayama HO, Kagawa S. Serum levels of soluble interleukin-2 receptor in renal cell carcinoma. *Urology.* 1998;51(1):145-149.
41. Pountain G, Hazleman B, Cawston TE. Circulating levels of IL-1beta, IL-6 and soluble IL-2 receptor in polymyalgia rheumatica and giant cell arteritis and rheumatoid arthritis. *Br J Rheumatol.* 1998;37(7):797-798.
42. Zekri AR, Alam El-Din HM, Bahnassy AA, et al. Serum levels of soluble Fas, soluble tumor necrosis factor-receptor II, interleukin-2 receptor and interleukin-8 as early predictors of hepatocellular carcinoma in Egyptian patients with hepatitis C virus genotype-4. *Comp Hepatol.* 2010:9(1):1.
43. Sheibani K, Winberg CD, van de Velde S, Blayney DW, Rappaport H. Distribution of lymphocytes with interleukin-2 receptors (TAC antigens) in reactive lymphoproliferative processes, Hodgkin's disease, and non-Hodgkin's lymphomas. An immunohistologic study of 300 cases. *Am J Pathol.* 1987;127(1):27-37.
44. Robb RJ, Rusk CM. High and low affinity receptors for interleukin 2: implications of pronase, phorbol ester, and cell membrane studies upon the basis for differential ligand affinities. *J Immunol.* 1986;137(1):142-149.
45. Sheu BC, Hsu SM, Ho HN, Lien HC, Huang SC, Lin RH. A novel role of metalloproteinase in cancer-mediated immunosuppression. *Cancer Res.* 2001;61(1):237-242.
46. Fluckiger AC, Garrone P, Durand I, Galizzi JP, Banchereau J. Interleukin 10 (IL-10) up-regulates functional high affinity IL-2 receptors on normal and leukemic B lymphocytes. *J Exp Med.* 1993; 178(5):1473-1481.

Incorporation of Biaryl Units into the 5′ and 3′ Ends of Sense and Antisense Strands of siRNA Duplexes Improves Strand Selectivity and Nuclease Resistance

Kayo Yoshikawa,[†] Aya Ogata,[†] Chiho Matsuda,[§] Michinori Kohara,[§] Hideo Iba,[||] Yukio Kitade,[†,‡] and Yoshihito Ueno*[,†,‡]

Department of Biomolecular Science, Faculty of Engineering, and United Graduate School of Drug Discovery and Medical Information Sciences, Gifu University, 1-1 Yanagido, Gifu 501-1193, Japan, Department of Microbiology and Cell Biology, The Tokyo Metropolitan Institute of Medical Science, 2-1-6, Kamikitazawa, Setagaya-ku, Tokyo 156-0057, Japan, and Division of Host-Parasite Interaction, Department of Microbiology and Immunology, Institute of Medical Science, The University of Tokyo, 4-6-1 Shirokanedai, Minato-ku, Tokyo 108-8639, Japan. Received July 5, 2010; Revised Manuscript Received November 30, 2010

Small interfering RNA (siRNA) is a noncoding RNA with considerable potential as a new therapeutic drug for intractable diseases. siRNAs can be rationally designed and synthesized if the sequences of the disease-causing genes are known. In this paper, we describe the synthesis and properties of siRNAs modified with biaryl units. We found that incorporation of biaryl units into the 5′ and 3′ ends of sense and antisense strands of siRNA duplexes improved strand selectivity and nuclease resistance.

INTRODUCTION

RNA interference (RNAi) is a biological process whereby double-stranded RNAs (dsRNAs) silence gene expression in a sequence-specific manner (*1*). Small RNAs, including small interfering RNA (siRNA) and microRNA (miRNA), are key intermediates in RNAi. They regulate gene expression through the RNA-induced silencing complex (RISC), which contains Argonaute proteins as core components. siRNAs hold considerable potential as new therapeutic drugs for intractable diseases, because they can be rationally designed and synthesized if the sequences of disease-causing genes are known (*2*–*6*).

One strand from an siRNA or miRNA duplex is selected and loaded onto RISC to become mature siRNA or miRNA. It has been suggested that RISC preferentially selects and incorporates one of two strands of the siRNA duplex, depending on its thermodynamic features. The strand with thermodynamically lower stability in its 5′-terminus (the guide strand) preferentially binds the RISC and becomes functional, whereas the other strand (the passenger strand) is degraded (*7*–*9*). However, it has recently become clear that strand selection does not always follow this rule (*1*–*14*). Recently reported siRNA studies demonstrated that modifying the 5′-terminus of one strand with 5′-*O*-methyl efficiently specifies its antisense strand to be loaded onto RISC despite thermodynamic disadvantages (*15*), because 5′-*O*-methyl inhibits phosphorylation of the 5′-terminus, which is an important factor for RISC loading (*16*–*20*).

We have reported the synthesis of DNAs containing biaryl units, **3** and **5**, which comprised benzene and naphthalene or pyrene residues (Figure 1). The biaryl units thermally and thermodynamically stabilized DNA/DNA duplexes (*21*). We have also succeeded in improving siRNA nuclease resistance by introduction of bis(hydroxymethyl)benzene (**1**) instead of thymidine at 3′-overhangs without reducing RNAi-inducing activity (*22*). From these results and background information, we planned the synthesis of siRNAs with biaryl units at the 5′ and 3′ ends of sense and antisense strands of siRNA duplexes, respectively. We expected that thermal and thermodynamic stabilities of the 5′ regions of siRNA sense strands would be increased by these biaryl modifications. Phosphorylation of the 5′ ends of sense strands, an important factor for RISC loading, was expected to be inhibited by biaryl protection of 5′-hydroxyls. We anticipated that these modifications would enhance RISC loading of antisense strands of siRNA duplexes, suppressing off-target effects induced by sense strands. We also anticipated improved nuclease resistance in biaryl-modified siRNAs, which is important for the therapeutic application of synthetic siRNAs.

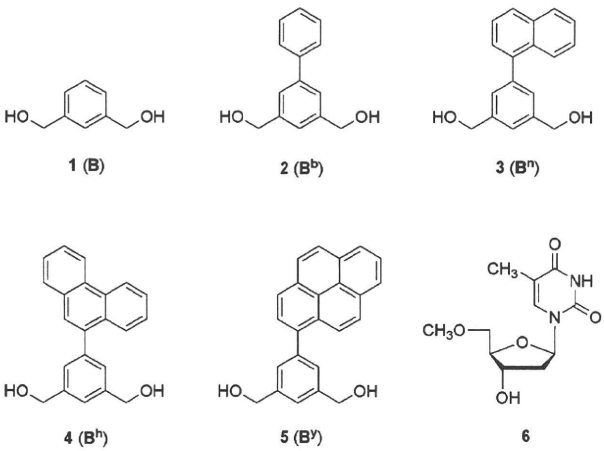

Figure 1. Structures of the aromatic compounds and modified nucleoside used in this study.

In this paper, we report the synthesis and properties of siRNA duplexes which carry biaryl units at the 5′ and 3′ ends of sense and antisense strands, respectively. We assessed the gene

* To whom correspondence should be addressed. Phone: +81-58-293-2639. Fax: +81-58-293-2794. E-mail: uenoy@gifu-u.ac.jp.
[†] Department of Biomolecular Science, Faculty of Engineering, Gifu University.
[‡] United Graduate School of Drug Discovery and Medical Information Sciences, Gifu University.
[§] The Tokyo Metropolitan Institute of Medical Science.
[||] The University of Tokyo.

10.1021/bc100301w
Published on Web 12/09/2010

Scheme 1[a]

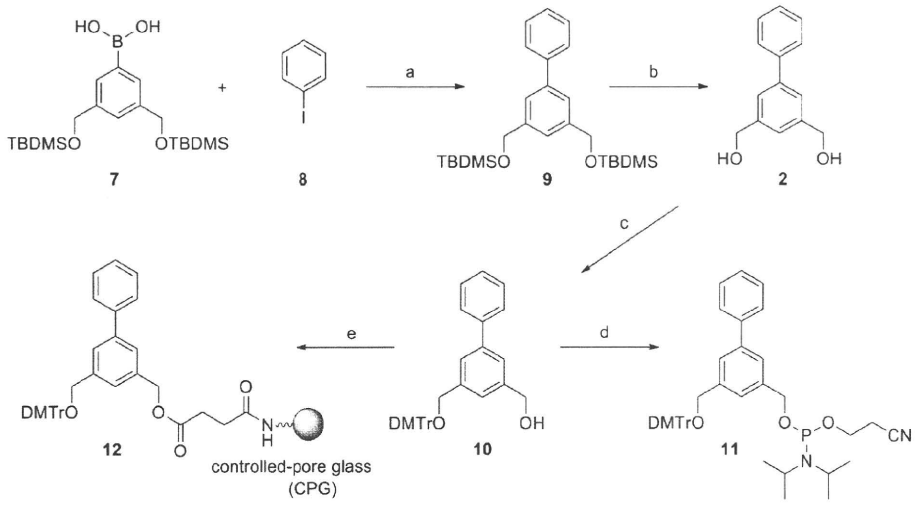

[a] Reagents and conditions: (a) $PdCl_2(dppf)\cdot CH_2Cl_2$, NaOH, THF/$H_2O$ (5:1 v/v), 65 °C, 24 h; (b) TBAF, THF, rt, 2 h, 93% from **7**; (c) DMTrCl, pyridine, rt, 4 h, 52%; (d) chloro(2-cyanoethoxy)(*N*,*N*-diisopropylamino)phosphane, *i*-Pr_2NEt, THF, rt, 1 h, 88%; (e) (1) succinic anhydride, DMAP, pyridine, rt, 24 h; (2) CPG, EDCI, DMF, rt, 48 h, 49 μmol/g loading amount.

Scheme 2[a]

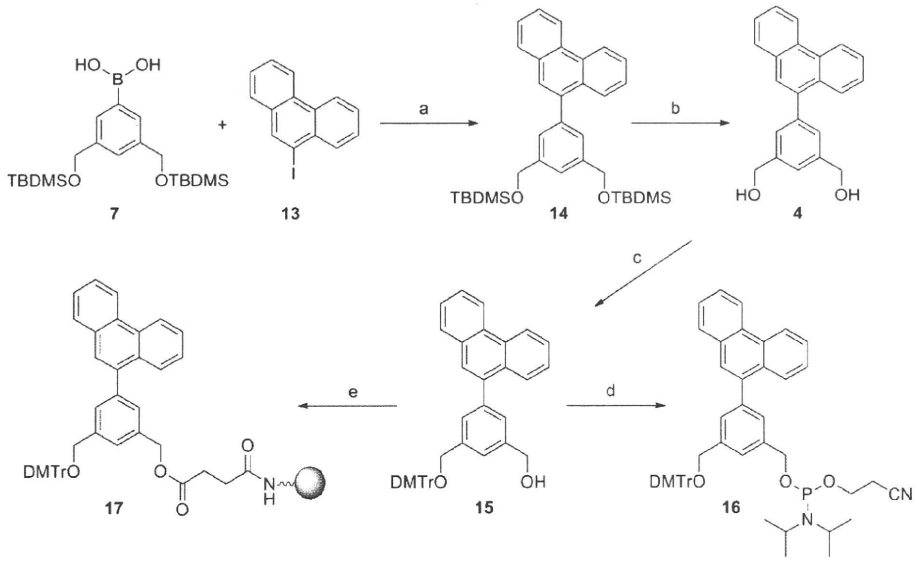

[a] Reagents and conditions: (a) $PdCl_2(dppf)\cdot CH_2Cl_2$, NaOH, THF/$H_2O$ (5:1 v/v), 65 °C, 24 h; (b) TBAF, THF, rt, 2 h, 60% from **7**; (c) DMTrCl, pyridine, rt, 3 h, 61%; (d) chloro(2-cyanoethoxy)(*N*,*N*-diisopropylamino)phosphane, *i*-Pr_2NEt, THF, rt, 1 h, 74%; (e) (1) succinic anhydride, DMAP, pyridine, rt, 24 h; (2) CPG, EDCI, DMF, rt, 48 h, 45 μmol/g loading amount.

silencing activities of the modified siRNAs by a dual-luciferase assay. We also assessed the nuclease-resistance of the modified siRNAs.

RESULTS AND DISCUSSION

Design and Synthesis of siRNAs. The Argonaute proteins are core components of RISC, which is responsible for mRNA cleavage in the RNAi pathway. The proteins are composed of PAZ, Mid, and PIWI domains. X-ray structural analysis and a nuclear magnetic resonance (NMR) study have revealed that the 3′-overhang region of a guide strand of siRNA is recognized by the PAZ domain and the 2-nucleotide (nt) 3′-overhang is accommodated by a binding pocket composed of hydrophobic amino acids (*23*−*26*). In order to estimate the appropriate size for biaryl units in the 3′-overhang region, we assessed the silencing activities of siRNAs which carried various types of biaryl units at the 3′-overhangs.

We assessed the biaryl units **2** ($\mathbf{B^b}$), **3** ($\mathbf{B^n}$), **4** ($\mathbf{B^h}$), and **5** ($\mathbf{B^y}$), comprising benzene and benzene, naphthalene, phenanthrene, or pyrene residues, to determine the appropriate size for the 3′-overhang regions. Phosphoramidites of **3** and **5** were synthesized according to a previously reported method (*21*). Phosphoramidites of **2** and **4** and solid supports carrying **2** or **4** were synthesized according to the methods shown in Schemes 1 and 2. An arylboronic acid derivative **7** was coupled with iodobenzene (**8**) in the presence of $PdCl_2(dppf)$ (dppf stands for 1,1′-bis(diphenylphosphanyl)ferrocene) at 65 °C; this coupling reaction produced the biaryl derivative **9**; subsequently, **9** was desilylated by treatment with tetra-*n*-butylammonium fluoride (TBAF) to give a 93% yield of biaryl unit **2.** One out of the two hydroxy groups of **2** was protected by a 4,4′-dimethoxytrityl (DMTr) group to give a 52% yield of mono-DMTr derivative **10**. **10** was phosphitylated by the standard procedure to produce the corresponding phosphoramidite **11** at